Tropical Cyclone Intensity Errors Associated with Lack of Two-Way Ocean Coupling in High-Resolution Global Simulations

COLIN M. ZARZYCKI

National Center for Atmospheric Research,[a] *Boulder, Colorado*

(Manuscript received 3 April 2016, in final form 23 August 2016)

ABSTRACT

Tropical cyclones (TCs), particularly those that are intense and/or slow moving, induce sea surface temperature (SST) reductions along their tracks (commonly referred to as cold wakes) that provide a negative feedback on storm energetics by weakening surface enthalpy fluxes. While computing gains have allowed for simulated TC intensity to increase in global climate models as a result of increased horizontal resolution, many configurations utilize prescribed, noninteractive SSTs as a surface boundary condition to minimize computational cost and produce more accurate TC climatologies. Here, an idealized slab ocean is coupled to a 0.25° variable-resolution version of the Community Atmosphere Model (CAM) to improve closure of the surface energy balance and reproduce observed Northern Hemisphere cold wakes. This technique produces cold wakes that are realistic in structure and evolution and with magnitudes similar to published observations, without impacting large-scale SST climatology. Multimember ensembles show that the overall number of TCs generated by the model is reduced by 5%–9% when allowing for two-way air–sea interactions. TC intensity is greatly impacted; the strongest 1% of all TCs are 20–30 hPa (4–8 m s^{-1}) weaker, and the number of simulated Saffir–Simpson category 4 and 5 TCs is reduced by 65% in slab ocean configurations. Reductions in intensity are in line with published thermodynamic theory. Additional offline experiments and sensitivity simulations demonstrate this response is both significant and robust. These results imply caution should be exercised when assessing high-resolution prescribed SST climate simulations capable of resolving intense TCs, particularly if discrete analysis of extreme events is desired.

1. Introduction

Sea surface temperature (SST) and tropical cyclones (TCs) are known to be intrinsically linked, with warm ocean waters providing heat and moisture that fuel the thermodynamic processes driving TCs (Emanuel 1986). Although SSTs have been shown to be an inadequate indicator of forecasted storm intensity for individual systems (Evans 1993), they do serve to provide an upper bound on the potential intensity of cyclones (Emanuel 1986; DeMaria and Kaplan 1994) and to constrain the geographic pattern and seasonal cycle of tropical formation (Gray 1968; Galvin 2008). While TCs are strongly dependent on the magnitude and spatial pattern of SSTs (e.g., Chauvin et al. 2006), they also have the capability to significantly impact upper ocean temperature (Price 1981). The most notable manifestation of this feedback is the formation of a negative SST anomaly (SSTA; also referred to as a TC's cold wake) along a TC's trajectory that persists from days to weeks following storm passage. TC-induced SSTAs form as a result of heat extraction and mixing processes in the upper ocean and may range anywhere from a fraction of kelvin to 10 K (e.g., Shay et al. 1992; Cione and Uhlhorn 2003; Price et al. 2008; Lin et al. 2009; Mei and Pasquero 2013). This SST reduction can have considerable impacts on the energy available for TC intensification and maintenance, primarily through reduced surface enthalpy fluxes (Bender et al. 1993; Schade and Emanuel 1999; Knutson et al. 2001; Cione and Uhlhorn 2003; D'Asaro et al. 2007).

As the capacity of computing clusters continues to grow, the horizontal resolutions of global atmospheric general circulation models (AGCMs) continue to increase. Higher horizontal resolution improves climate simulations in many ways, with one striking example being TCs (Walsh et al. 2015). Models integrated at

[a] The National Center for Atmospheric Research is sponsored by the National Science Foundation.

Corresponding author address: Colin M. Zarzycki, National Center for Atmospheric Research, P.O. Box 3000, Boulder, CO 80307.
E-mail: zarzycki@ucar.edu

DOI: 10.1175/JCLI-D-16-0273.1

standard grid spacings of 1° and coarser struggle greatly in the representation of TCs, either producing highly underresolved storms or failing to simulate them altogether (Bengtsson et al. 2007; Daloz et al. 2012b; Zarzycki and Jablonowski 2014; Wehner et al. 2014). However, recent work has shown that high-resolution AGCMs [high resolution here being defined as 0.5° latitude/longitude (~56 km) and finer] have demonstrated the capability to produce more realistic storm counts and intensities (Oouchi et al. 2006; Bengtsson et al. 2007; Zhao et al. 2009; Murakami et al. 2012; Manganello et al. 2012; Satoh et al. 2012; Strachan et al. 2013; Zarzycki and Jablonowski 2014; Wehner et al. 2015).

Although the two-way interaction between SSTs and TCs is important, the vast majority of high-resolution, global, AGCM simulations are integrated using fixed (sometimes referred to as prescribed) SSTs as a lower (surface) boundary condition. This treats the ocean as a potentially infinite heat source (or sink) with respect to the atmosphere. There are a few reasons motivating this "data ocean" setup. One practical one is the avoidance of the significant computational cost required when coupling a high-resolution AGCM to a similarly high-resolution dynamical ocean model. Additionally, and of distinct importance to TCs, dynamic ocean models frequently suffer from regional SST biases, which may impact the spatial and temporal distribution of simulated cyclogenesis. For example, the majority of CMIP5 models produce broad, cold SST biases in the North Atlantic (Wang et al. 2014). In a high-resolution (0.25° for atmosphere and 0.1° for ocean) coupled simulation where this bias occurs, Atlantic TC activity is shown to be highly suppressed relative to observations (Small et al. 2014), making this configuration inadequate for analysis of realistic TC impacts. This poor climatological TC representation is due to these SST biases, as simulations using the same AGCM with prescribed SSTs produce very realistic spatial patterns of TCs (Bacmeister et al. 2014; Zarzycki and Jablonowski 2014; Wehner et al. 2014; Reed et al. 2015). Similar issues with regional ocean surface temperature biases and TC activity have been noted in other coupled studies with coarser atmospheric model grid spacings of 50 km and larger (Scoccimarro et al. 2011; Daloz et al. 2012a; Bell et al. 2013; Kim et al. 2014; Li et al. 2016). Last, the use of fixed SST configurations is partially due to inertia. The coarser grid spacings of the previous generation of AGCMs were unable to resolve intense, small-scale features (such as TCs) capable of impacting ocean SSTs, thereby making the assumption of prescribed SSTs more valid [see the underestimation of TC-induced SSTAs in an ocean model using coarse ERA-Interim forcing (~79-km grid spacing) in Jourdain et al. (2014)].

Given the commonly used practice of prescribing SSTs, it is plausible that TCs simulated in atmosphere-only GCM experiments suffer from an intensity bias resulting from the lack of reduced SSTs underneath the storm core. Since this feedback disproportionately impacts stronger storms (Lloyd and Vecchi 2011; Mei and Pasquero 2013), it is likely to be most noticeable in the tail of the TC distribution (most intense storms). Correspondingly, this bias has certainly been rather small with older AGCMs that were only able to simulate weaker TCs as a result of insufficient horizontal resolution (e.g., Bengtsson et al. 2007). Coupled limited-area models (LAMs) with simplified configurations have demonstrated this feedback using higher spatial resolution than these low-resolution GCMs (Knutson et al. 2001; Jullien et al. 2014). However, LAMs require boundary conditions, which can deleteriously impact TC activity (Landman et al. 2005; Caron and Jones 2012), and do not allow for global teleconnections, which may be important for both the atmosphere (Archambault et al. 2013) and ocean (Scoccimarro et al. 2011), thereby making global models a preferred option where possible. Since experimental high-resolution AGCMs are demonstrating the capability to simulate TCs that approach maximum intensities found in observations (Manganello et al. 2012; Murakami et al. 2012; Strachan et al. 2013; Zarzycki and Jablonowski 2014; Wehner et al. 2015), the lack of two-way SST coupling in these simulations is likely to grow more problematic with future generations of global models.

With models capable of simulating such strong TCs, it is prudent to investigate this phenomenon. This paper seeks to quantify this bias in a mean sense with respect to TC climatology in high-resolution climate simulations. It differs from previous work in that an ocean model of intermediate complexity is applied, maintaining core aspects of the prescribed SST (correct SST climatology) and coupled dynamic ocean model (air–sea surface energy closure) frameworks that are crucial for the correct simulation of TCs in a global climate model. To achieve this, an idealized computationally efficient slab ocean parameterization designed to approximate observed TC cold wakes is coupled to a global model. Since this slab ocean is relaxed to a background prescribed SST state, the climatological large-scale surface forcing is correct. This allows for the isolation of SSTA impacts on TC climatology, an analysis not available with traditional slab ocean or fully coupled climate simulations. An AGCM that has previously demonstrated the capability of simulating realistic, intense TCs is used to generate larger SSTAs that are in line with historical observations. The combination of realistic TC intensities and realistic cold wakes allows for an assessment of the average intensity differences between models with one-way (inactive) and

TABLE 1. Particular model components and configuration used in this study.

Component	Configuration
Earth system	CESM, version 1.3.17 (Hurrell et al. 2013)
Atmosphere	CAM, version 5.3.65 (Neale et al. 2012)
Dynamical core	Spectral element (Dennis et al. 2012)
Base resolution	1° (111 km)
Fine resolution	0.25° (28 km)
Time step	900 s (physics) and 38 s (dynamics)
Land	Community Land Model, version 4.0 (Oleson et al. 2010)
Ocean	Prescribed (HadISST; Hurrell et al. 2008) and slab model (this study)
Ice	Prescribed (HadISST)

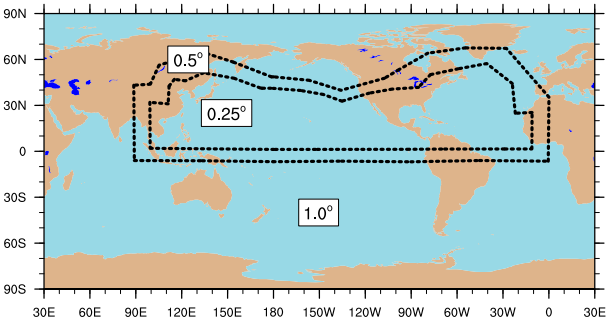

FIG. 1. Grid used in this study. Grid spacing inside the innermost black dashed contour is approximately 0.25° (28 km), and the base resolution outside the outermost black dashed contour is 1° (111 km). A transition region of 0.5° (56 km) resolution separates the two.

two-way (active) SST coupling and, correspondingly, potential errors that may be introduced in TC climatology by neglecting surface energy balance.

This manuscript is outlined as follows. Section 2 discusses the model setup, slab ocean, experimental configuration, and tracking methodology. The simulation results are compared to observational records of SSTAs in section 3. The differences between prescribed SST experiments and those permitting TC cold wakes are explored in section 4. Section 5 describes some sensitivity configurations of the model setup, and section 6 discusses the implications for these results and suggests future avenues of research.

2. Experimental design

a. Model setup

The model used here is the National Science Foundation (NSF)/U.S. Department of Energy (DOE) Community Atmosphere Model (CAM), version 5 (CAM5; Neale et al. 2012), which is the atmospheric component of the Community Earth System Model (CESM; Hurrell et al. 2013). In particular, the variable-resolution option of the spectral element (CAM-SE) dynamical core is used. CAM-SE provides robust conservation properties in addition to attractive scaling on massively parallel computing systems (Taylor et al. 1997; Taylor and Fournier 2010; Dennis et al. 2012; Evans et al. 2013). CAM-SE is also capable of performing integrations on variable-resolution grids (Zarzycki et al. 2014), which have been shown to produce simulations of realistic global climates while enhancing the representation of small-scale features within the refined region (Zarzycki et al. 2015). Variable-resolution grids allow for a significant computational cost reduction (compared to globally uniform high-resolution simulations), an aspect highly beneficial in TC studies since storms follow well-defined regional genesis and track patterns (Zarzycki and Jablonowski 2014). Particular details of the model configuration are found in Table 1. Readers are referred to Zarzycki and Jablonowski (2014) for further specifics regarding this setup for use in TC climate studies.

The variable-resolution grid used is shown in Fig. 1. The base resolution is approximately 1° (111 km). Horizontal refinement to 0.25° (28 km) resolution is located over the North Atlantic and North Pacific Ocean basins, with a band of 0.5° (56 km) grid spacing providing a transition region between the inner refinement and the base grid. The high-resolution nest is generated using the spherical quadrilateral mesh generator utility (SQuadGen; Guba et al. 2014) and is defined by refining over regions of historical TC activity in the Northern Hemisphere as recorded in the International Best Track Archive for Climate Stewardship (IBTrACS; Knapp et al. 2010) dataset. This mesh contains 30% of the grid cells of a globally uniform 0.25° grid, resulting in a factor of 3.3 speedup because of reduced computational requirements in the regions outside of the domains of interest (i.e., given identical computational allocations, the variable-resolution setup produces 3.3 months of simulated data for every 1 month from a uniform high-resolution setup).

Three experimental configurations are defined. The first (FIXED) uses prescribed SSTs and ice cover concentrations (ICCs) for surface forcing. These quantities vary in time, but the ocean is only coupled to the atmosphere in one direction (passing surface fluxes to the atmosphere's lowest model levels). This configuration is identical to those used in the majority of high-resolution, multidecadal TC assessments (Walsh et al. 2015). The other two configurations (SLAB1 and SLAB2) employ the slab ocean discussed in the following section.

All forcings, including SSTs, ICCs, aerosol and gaseous species concentrations, and solar insolation are 1981–2000 climatological means. The model is first spun up with prescribed SSTs for 16 months to generate

balanced atmosphere and land states on 1 May, which serve as initial conditions. Ensemble members for each configuration are then generated by adding 1% random white note perturbations to the atmospheric temperature, moisture, and surface pressure fields at the gridcell level. Each member is integrated for 7 months. The first month is discarded for spinup, limiting analysis to between 1 June and 1 December. Comparison of root-mean-square differences of various dynamical quantities, such as temperature, kinetic energy, and precipitation, show that members achieve maximum spread at approximately 21 days (not shown), indicating that this framework produces uncorrelated ensembles beyond the first month. Each of the three base configurations is composed of 25 Northern Hemisphere tropical cyclone seasons (therefore 450 total months after spinup are discarded).

b. Slab ocean formulation

A simple, inexpensive way to allow for two-way feedbacks between the atmosphere and ocean is the implementation of a slab ocean. A slab ocean (sometimes referred to as a ''single mixed layer ocean'' or ''thermodynamic ocean'') uses a single-level, column framework to allow for an approximation of energy balance at the atmosphere–ocean interface. The traditional formulation for the rate of change of slab ocean sea surface temperature ($\partial \mathrm{SST}/\partial t$) is

$$\frac{\partial \mathrm{SST}}{\partial t} = \frac{1}{\rho_o c_p h} F_{\mathrm{net}}, \tag{1}$$

where ρ_o is the density of seawater, c_p is the heat capacity of seawater, h is a climatological mixed layer depth, and F_{net} is the net heat flux into the ocean. Because of the lack of horizontal connectivity (and therefore ocean current representation), climatological SSTs in real-world simulations using a slab ocean are poorly reproduced, especially in areas where observed SSTs deviate from a zonal structure. This issue has been addressed in ways such as the addition of spatially dependent heat to the bottom of the mixed layer (Kiehl et al. 2006; Bitz et al. 2012) or a prescribed horizontal diffusion empirically derived from observations (Donnadieu et al. 2006).

TC cold wakes are formed by three primary processes: extraction of heat from the surface via latent and sensible heat fluxes, turbulent upwelling of cooler water from below the mixed layer, and horizontal advection of surface water due to Ekman pumping (Ginis 2002; Vincent et al. 2012a). Turbulent mixing accounts for most of the cooling under the majority of TCs, contributing to approximately 70%–90% of an intense storm's cold wake (Price 1981; D'Asaro et al. 2007; Huang et al. 2009; Vincent et al. 2012a). While typically a lesser contributor, surface fluxes are the primary surface cooling mechanism for weaker cyclones and contribute to SST cooling outside the storm core (Morey et al. 2006). Advection generally plays the smallest role in cold wake formation; however, its impact may become equal to (or surpass) that of flux-induced cooling for very intense cyclones (although it remains far weaker than cooling resulting from mixing) (Vincent et al. 2012a).

Therefore, since turbulent mixing and upwelling contribute significantly to TC-induced SSTAs, Eq. (1) will greatly underestimate the cold wake produced by storms, particularly for stronger TCs. This problem can be addressed through the addition of terms to mimic these cooling processes in an empirical sense. Assuming that the magnitude of TC-induced cooling is related to surface wind stress, mixed layer depth, and the temperature gradient in the near-surface ocean (Vincent et al. 2012a), a modification to Eq. (1) can be defined as follows:

$$\frac{\partial \mathrm{SST}}{\partial t} = \frac{1}{\rho_o c_p h} F_{\mathrm{net}} - X_{\mathrm{cool}} R_{\mathrm{cool}} \left(\frac{\mathrm{SST} - T_{\mathrm{deep}}}{\Delta T_o} \right) \left(\frac{h_o}{h} \right) + \frac{1}{\tau} (\mathrm{SST}_{\mathrm{clim}} - \mathrm{SST}). \tag{2}$$

The second term on the right-hand side of Eq. (2) represents an empirical parameterization of cooling induced by turbulent mixing and advective processes under a TC. The variable X_{cool} is a weighting that is a function of 10-m surface wind speed u_{10}, and R_{cool} is a normalized base cooling rate; T_{deep} is a generalized deep water temperature, and ΔT_o is a scaling temperature difference between the surface and deep water. This scaling acts to impart stronger cooling where ocean stratification is larger, as well as to restrict cooling to tropical latitudes where TCs are most prevalent (e.g., Schade and Emanuel 1999; Emanuel 2015). In the final component, h_o is a constant mixed layer reference depth, and h is a climatological mixed layer depth that varies spatially but not temporally. This mixed layer term produces more cooling with lower values of h since TCs are more readily able to cool SSTs in regions of shallower mixed layers (e.g., Vincent et al. 2012b).

The weighting X_{cool} is defined as follows:

$$X_{\mathrm{cool}} = K[1 + e^{-\alpha(u_{10} - u_{10,\mathrm{ref}})}]^{-1}. \tag{3}$$

A value of 1.0 for X_{cool} (at a given u_{10}) provides a cooling rate equal to R_{cool} at that grid cell (that is then scaled appropriately depending on the SST and mixed layer depth). Two different formulations for X_{cool} are assessed. The first is a simple logistic function, referred to as SLAB1, where α is equal to 0.5, $u_{10,\mathrm{ref}}$ is equal to 30 m s^{-1}, and K is equal to 1. As seen in Fig. 2, this

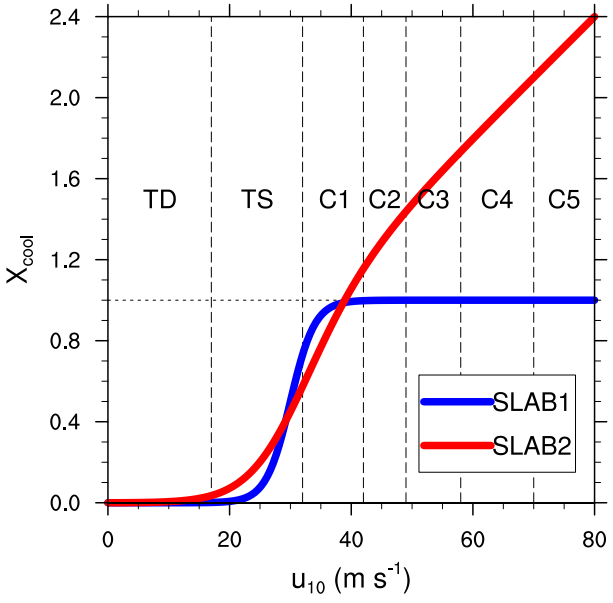

FIG. 2. Forcing functions X_{cool} for both the SLAB1 and SLAB2 versions of the parameterization in Eq. (2) as a function of u_{10}. Saffir–Simpson intensity bins are overlaid with vertical dashed black lines.

function induces little cooling at low wind speeds, but rapidly saturates above 35 m s^{-1}. This forcing therefore assumes that once TC intensity surpasses a specific threshold, turbulence-induced cooling becomes virtually maximized for a particular location, reproducing observed drag saturation (Powell et al. 2003; Donelan et al. 2004). This behavior is also in line with the results of Lloyd and Vecchi (2011) and Mei and Pasquero (2013) (among others), who found that the magnitudes of cold wakes were approximately equal once TC surface winds surpassed 35–40 m s^{-1}.

The second formulation is referred to as SLAB2 where α is equal to 0.2, and K is equal to $u_{10}(k_{ref}/u_{10,ref})$, where k_{ref} is set to 0.9, and $u_{10,ref}$ remains 30 m s^{-1}. This function applies a linear forcing K in combination with the logistic function, leading to the weighting seen in Fig. 2. Like SLAB1, the logistic component results in very little mixing at low wind stresses. However, the linear term addition allows for TC-induced cooling to continue to increase as u_{10} increases, based on idealized theory where friction velocity increases monotonically with surface wind speed. This results in an approximate doubling in forcing for $u_{10} = 60$ m s^{-1}, relative to SLAB1.

The third and final term in Eq. (2) is a Newtonian relaxation to climatological SSTs, where τ is a relaxation time scale, and SST_{clim} is the climatological SST and relaxation state. This ensures that the mean SSTs in configurations utilizing the slab ocean setup are consistent with observed climatological SSTs (SST_{clim}) and is used in lieu of an additional spatially dependent flux correction to the parameterization. This relaxation is chosen since previous work assessing observed SSTAs in response to TC passage has demonstrated that SST recovery is generally exponential, with an *e*-folding time of approximately 5–20 days (e.g., Price et al. 2008; Jansen et al. 2010; Dare and McBride 2011; Mei and Pasquero 2013). SST_{clim} contains an optional, linearly added, correction factor on the order of 0.1 K, which is derived from simplified tuning experiments in order to more closely match observed SSTs. The background SSTs [SST_{clim} in Eq. (2)] that the slab ocean is relaxed toward are the same as in the FIXED forcing file in order to produce near-identical large-scale climatologies between all three ensemble configurations. Default values for all constants are listed in Table 2.

TABLE 2. Constants for slab ocean parameterization used in this study.

Parameter	Description	Value
ρ_o	Density of seawater.	1026 kg m^{-3}
c_p	Specific heat of seawater.	3996 J kg^{-1} K^{-1}
T_{deep}	Deep water temperature.	271 K
ΔT_o	Scaling temperature gradient.	27 K
τ	Newtonian SST relaxation time scale.	8 days
h_o	Scaling mixed layer depth.	30 m
R_{cool}	Base cooling rate.	4.7 K day^{-1}

c. *Tracking methodology*

Individual TCs are tracked using TempestExtremes software (Ullrich and Zarzycki 2016). A brief overview of the technique used is presented here, although a more comprehensive discussion of the general procedure for detecting TCs can be found in Zarzycki and Jablonowski (2014) (note that the parameter values are slightly different in this study). First, candidate storms are detected at 6-h time intervals by ensuring that a sea level pressure (SLP) minimum is surrounded by a closed contour of SLP 2 hPa greater than the minimum within 2° radius. This is defined as the TC center. A geopotential thickness maximum between the 300- and 500-hPa levels is used as a thermal criterion to eliminate non-warm-core storms. This thickness maximum must occur within 1° radius of the SLP minimum and be enclosed by a ring of thickness 10 m less than the maximum that fully lies within 5° radius of the maximum. Candidate cyclones are then stitched together in time, with storms needing to have surface (10 m) winds greater than 17.5 m s^{-1} (corresponding to the WMO tropical cyclone definition) for 2 days (not necessarily consecutive). The 10-m winds are obtained by reducing lowest model level (~60 m) winds to 10 m using the logarithmic technique described

TABLE 3. Saffir–Simpson intensity scale.

S–S category	Wind speed			
	$m\,s^{-1}$	kt	$mi\,h^{-1}$	$km\,h^{-1}$
Tropical depression (TD)	<17	<34	<38	<62
Tropical storm (TS)	18–32	35–63	39–73	63–118
Category 1 (C1)	33–42	64–82	74–95	119–153
Category 2 (C2)	43–49	83–95	96–110	154–177
Category 3 (C3)	50–58	96–112	111–129	178–208
Category 4 (C4)	58–70	113–136	130–156	209–251
Category 5 (C5)	≥70	≥137	≥157	≥252

in Zarzycki and Jablonowski (2014). The terms 10-m winds and surface winds are used interchangeably for the remainder of this manuscript. Storm translational speed is restricted to 20.5 $m\,s^{-1}$ (74 $km\,h^{-1}$), and separate trajectories that terminate and begin within 12 h and 8° radius of one another are merged to eliminate double counting of broken tracks. Cursory uncertainly quantification shows that relatively little sensitivity exists in choice of values for threshold criteria, particularly for more intense TCs (not shown). This agrees with both Walsh et al. (2007) and Zhao et al. (2009) and implies that the exact tracking technique used is not critical to the results of this particular study, since the strongest SSTAs are associated disproportionally with the most intense TCs. Storm intensities are binned by Saffir–Simpson (S–S) TC intensity classes (Simpson 1974), defined in Table 3.

SSTAs associated with tracked TCs in the two slab configurations are calculated using a Lagrangian composite method, similar to that described in Lloyd and Vecchi (2011). In this method, SSTAs (defined as SST minus SST_{clim}) are sampled using each 6-h storm location. Sampling is performed daily at a particular TC center location starting at 20 days prior to storm passage and ending at 40 days following storm passage. Unless otherwise specified, the SSTA at a particular time and location is calculated as the average over a 1° × 1° grid box.

All trajectories for TCs in the FIXED, SLAB1, and SLAB2 runs are shown in Fig. 3. The spatial distribution of TCs is well simulated, with cyclones originating in the North Atlantic, eastern Pacific, and western Pacific Ocean basins. The greatest number of TCs occurs in the western Pacific along with a higher frequency of intense TCs, in accordance with observations (Gray 1968). A high density of weaker cyclones forms in lower latitudes in the eastern Pacific. Storms generally form in the eastern and central portions of the Atlantic basin and

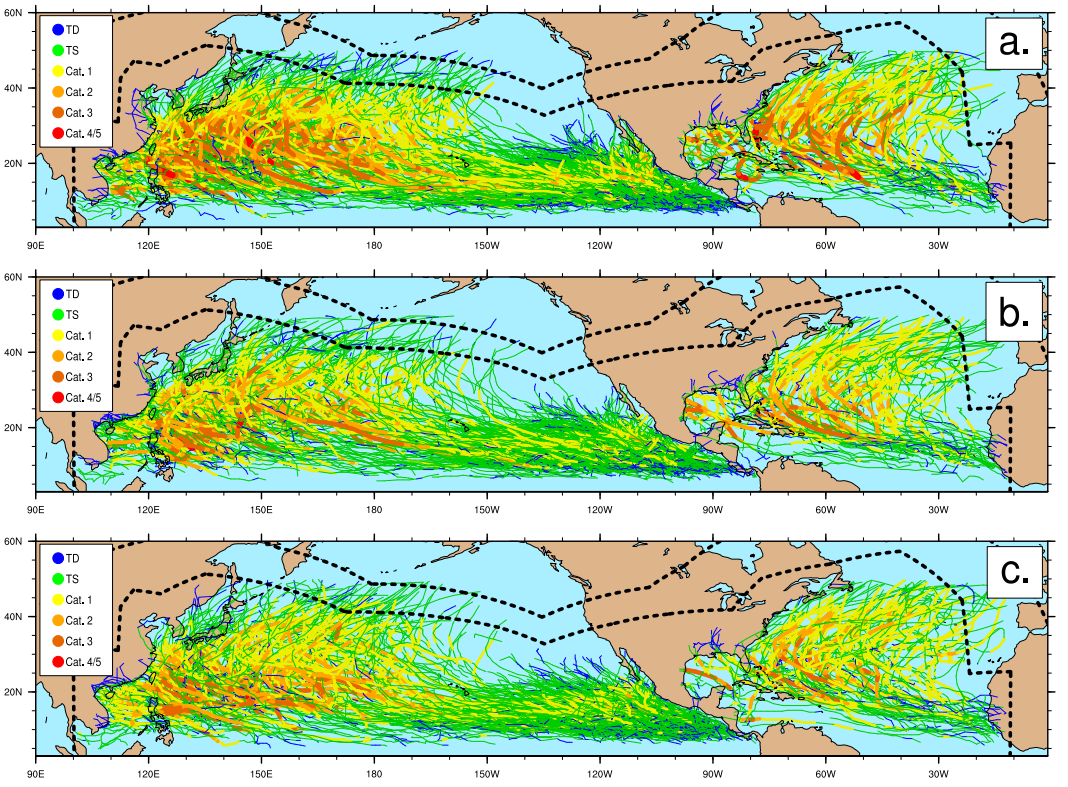

FIG. 3. TC trajectories for (a) FIXED, (b) SLAB1, and (c) SLAB2 configurations. Tracks encompass all 25 years of each set of simulations and are color coded by storm intensity as measured by the Saffir–Simpson scale.

track westward at lower latitudes, with the majority recurving to the east at mid-to-high latitudes.

To validate that the sample pattern of TCs generated by the configurations are similar, Pearson product-moment coefficients of linear correlation are computed over ensemble cumulative cyclone track density maps at 5° × 5° resolution. These correlation coefficients may be centered (Santer et al. 1993) or uncentered (Barnett and Schlesinger 1987), with the primary difference in application being that the centered method removes the global mean, whereas the uncentered method does not. Centered (uncentered) correlation coefficients are 0.97 and 0.97 (0.98 and 0.98) between FIXED and SLAB1 and FIXED and SLAB2, as well as 0.98 (0.99) between SLAB1 and SLAB2. Therefore, the TC samples generated in all three configurations (Fig. 3) are highly similar, confirming that this method will allow for direct isolation of the SST feedback on TC intensity.

3. Comparison of slab ocean cold wakes with observations

Before attempting to quantify the impact of neglecting sea surface interactions under TCs in high-resolution climate simulations, the slab ocean configuration described in section 2b needs to be validated.

An example of simulated TC cold wakes is displayed in Fig. 4. Instantaneous snapshots of SSTA (blue shading; K) are shown overlaid with 10-m wind speed (red–yellow shading; $m\,s^{-1}$). In the North Atlantic, two TCs are apparent in the top panel of Fig. 4, with both leaving trailing cold wakes over the next 5 days as they move toward higher latitudes (Fig. 4, top three panels). These cold wakes then slowly dissipate for the bottom two panels of Fig. 4 (through 21 September). Three other cyclones (two in the eastern Pacific and one in the North Atlantic) can be seen in the bottom panels of Fig. 4. The magnitude of the induced SSTA is primarily a function of translation speed, size, and strength of the cyclone. For example, the third (southernmost) TC in the North Atlantic produces a strong cold wake (exceeding −2 K) because of its high intensity and slow translational speed, while the westernmost cyclone in the eastern Pacific produces a smaller, weaker wake, since the TC is less intense and faster moving. The general spatial pattern and evolution of the cold wakes are well matched to those in both observations (e.g., Cione and Uhlhorn 2003; D'Asaro et al. 2007) and modeling case studies (e.g., Bender and Ginis 2000).

Table 4 compares recent studies that quantify the magnitude of TC SSTAs with the cold wakes produced in this study. Shown is the mean value of the maximum (absolute value) SSTA (1–2 days following TC passage)

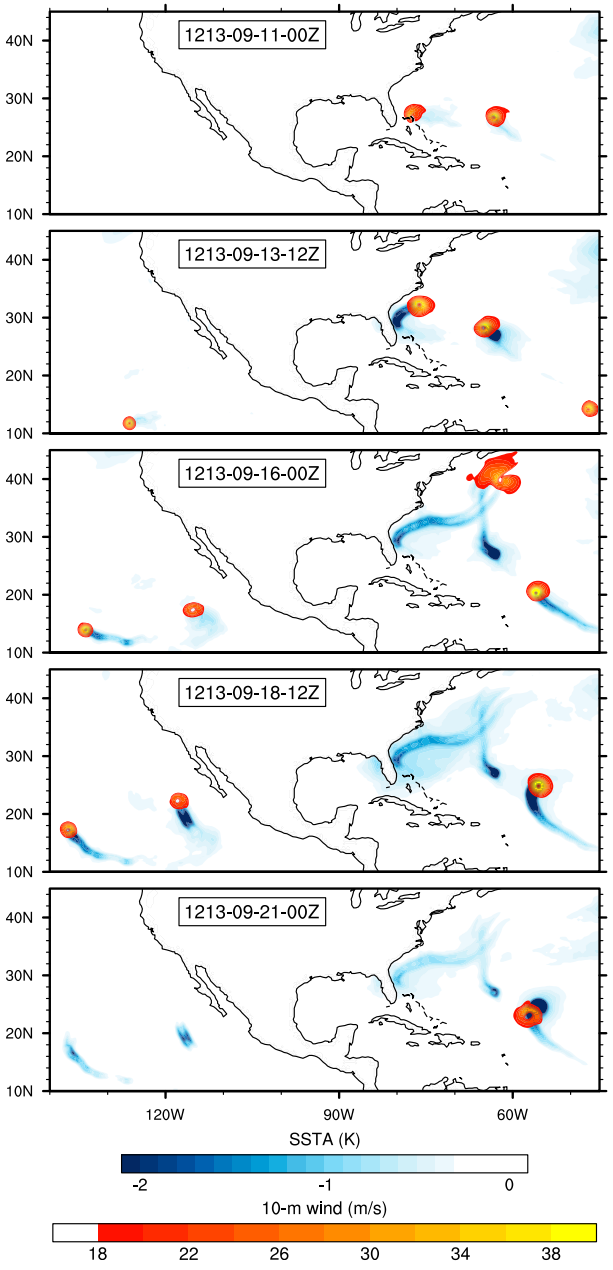

FIG. 4. Snapshot of the evolution of multiple cold wakes during September of ensemble member 13 in the SLAB1 configuration. SSTAs are shaded in blue and overlaid with u_{10} (red–yellow shading). (top)–(bottom) The elapsed time between each panel is 60 h.

for a particular intensity bin of TCs. Note the large range of gridbox "footprints" ΔX used to calculate cold wakes in the various studies, as well as the multitude of satellite products used to estimate SST. Mei and Pasquero (2013) found that SSTAs for stronger TCs can, on average, increase by a little more than 1 K in magnitude by varying the footprint from 9° × 9° to 1° × 1° as a result of the maximum cooling being constrained to within

100 km or so of the center of the TC. Therefore, attention was paid to recalculating SSTAs in this study for a particular ΔX in order to facilitate as similar a comparison as possible.

In general, simulated SSTAs here fall between the various observational estimates, with average cooling (for both SLAB1 and SLAB2) being slightly stronger than in Hart et al. (2007) and Lloyd and Vecchi (2011), approximately equal to Dare and McBride (2011) and Vincent et al. (2012a), and slightly weaker than Mei and Pasquero (2013). Mei and Pasquero (2013) hypothesized that earlier published SSTAs may be underestimated because of the impact of heavy rains on satellite SST retrieval. Regardless, these results demonstrate that the technique applied here provides a realistic magnitude signal. An analysis aimed at testing the sensitivity of the results to the spread in this data is discussed later.

Figure 5a shows the time series of the mean SSTA associated with TC passage (all storms) for all members in each SLAB configuration. Day 0 defines the time when the TC center is directly over the grid box of interest. The general shape of a sharp decline during storm passage (with SSTA maximized at +1–2 days) followed by an exponential recovery is well matched to the observational results of Hart et al. (2007, their Fig. 5), Dare and McBride (2011, their Fig. 5), and Mei and Pasquero (2013, their Fig. 12). Figures 5b and 5c show the results for only-hurricane-strength storms ($>33\,m\,s^{-1}$). The storms are broken into two classifications: fast-moving storms (Fig. 5b; translation speed $\geq 5\,m\,s^{-1}$) and slow-moving storms (Fig. 5c; translation speed $<5\,m\,s^{-1}$). Observations for various S–S intensity categories of slow-moving hurricanes from Lloyd and Vecchi (2011, their Fig. 3) are overlaid using green lines in Fig. 5c. In agreement with observations, slow-moving TCs produce larger SSTAs because of the increased residence time of surface forcing (winds) over a given location. Figure 5c also highlights good agreement between the model and observations in terms of both the maximum cold wake magnitude as well as the shape and time scale of the recovery.

Figure 6 shows the temporal evolution of the mean cross-track SSTA (hurricanes only) for the SLAB1 configuration. While not shown, the SLAB2 results are highly similar in both spatiotemporal evolution and magnitude. The model produces a realistic spatial response, with the maximum SSTA occurring to the right side of the storm (recall that all storms are in the Northern Hemisphere). Both observational (e.g., D'Asaro et al. 2007; Mei and Pasquero 2013) and modeling (e.g., Bender et al. 1993; Vincent et al. 2012a) studies have demonstrated this result, which primarily arises from asymmetric surface forcing due to the TCs forward translational vector being added to the cyclonic (rotational) wind component on the right side of the storm (Hazelworth 1968). However, this asymmetry is still likely somewhat underrepresented in this framework because of the lack of resonant effects between surface winds and inertial currents (Samson et al.

TABLE 4. Comparison of mean maximum SST response to TC passage from this study compared to recent observational assessments. The ΔX is the footprint (size of grid box) the SSTA (K) was taken over. Response is binned by S–S intensity category (left column) and includes all storms (AS), TD, TS, and various categories of hurricanes (see Table 3). (Footnotes include years included in observations as well as datasets used to estimate SST.)

	Obs	This study	
	Hart et al. (2007)[a]	SLAB1	SLAB2
ΔX	5° × 5°	5° × 5°	5° × 5°
TS	−0.30	−0.18	−0.28
C1–C3	−0.50	−0.63	−0.78
C3–C5	−0.56	−1.01	−1.11
	Dare and McBride (2011)[b]		
ΔX	0.25° × 0.25°	0.25° × 0.25°	0.25° × 0.25°
TD	−0.70	−0.13	−0.20
TS	−1.00	−0.26	−0.41
C1–C2	−1.37	−1.25	−1.37
C3–C5	−1.41	−2.02	−2.09
	Lloyd and Vecchi (2011)[c]		
ΔX	1° × 1°	1° × 1°	1° × 1°
AS	−0.85	−0.53	−0.68
TS	−0.59	−0.27	−0.44
C1	−1.05	−1.17	−1.30
C2	−1.31	−1.98	−1.99
C3	−1.36	−2.09	−2.16
C4	−1.28	−2.05	−1.86
	Vincent et al. (2012a)[d]		
ΔX	Radius ~200 km	3.6° × 3.6°	3.6° × 3.6°
TD	−0.25	−0.12	−0.18
TS	−0.71	−0.22	−0.34
C1	−1.11	−0.72	−0.89
C2	−1.42	−1.22	−1.31
C3	−1.42	−1.34	−1.44
C4	−1.32	−1.50	−1.15
	Mei and Pasquero (2013)[e]		
ΔX	5° × 5°	5° × 5°	5° × 5°
AS	−0.72	−0.29	−0.40
TD	−0.38	−0.11	−0.16
TS	−0.71	−0.18	−0.28
C1–C2	−1.17	−0.61	−0.76
C3–C5	−1.45	−1.01	−1.11
C1–C5	−1.27	−0.63	−0.78

[a] Study used Reynolds SST data (1985–2001). Data are from their Fig. 5.
[b] Study used Reynolds SST data (1981–2008). Data are from their Fig. 10.
[c] Study used TRMM Microwave Imager data (1998–2007). Data estimated from their Tables 1 and 2 and Fig. 4.
[d] Study used blend of TRMM Microwave Imager and AMSR-E data (1998–2007). Data are from their Fig. 6, and data presented represent median response.
[e] Study used TRMM Microwave Imager data (1997–2009). Data are from their Table 2.

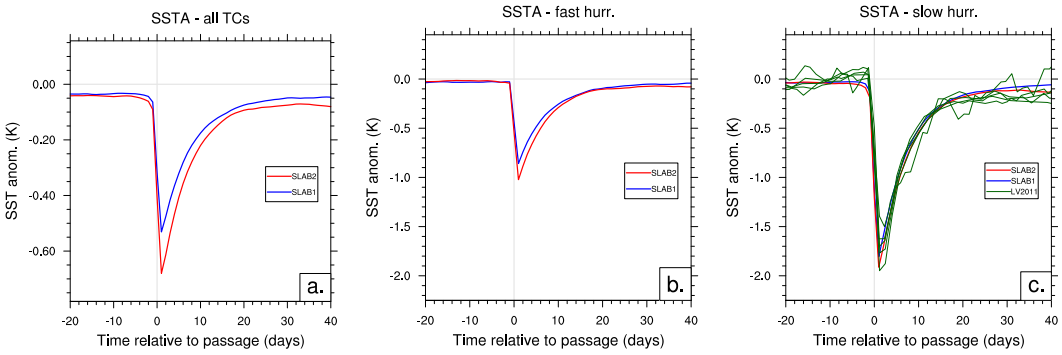

FIG. 5. SST response at fixed locations before, during, and after TC passage for SLAB1 and SLAB2 configurations as measured by a 1° × 1° grid box centered at the storm center. (a) The average response to all TCs and only-hurricane-strength ($u_{10} > 33\,\mathrm{m\,s^{-1}}$) storms are shown: (b) fast-moving storms (translational speed $\geq 5\,\mathrm{m\,s^{-1}}$) and (c) slow-moving storms ($<5\,\mathrm{m\,s^{-1}}$). The observed SST responses for multiple categories of hurricanes published in Lloyd and Vecchi (2011) for slow-moving hurricanes using the same 1° × 1° SST footprint are shown as thin green lines in (c) for reference. Note the difference in *y*-axis scale in (b) and (c).

2009). As previously seen in Fig. 5, the peak cooling occurs 1–2 days following the passage of the TC center. The onset of cooling also agrees with observational studies (e.g., Lloyd and Vecchi 2011; Mei and Pasquero 2013) and is evident a day or so prior to storm passage as a result of the leading edge of the cyclone producing cooling through enthalpy flux extraction in the outer portion of the wind field. Since the column-based slab ocean lacks simulated inertial effects, the center of the cold wake does not drift toward the left (in the Northern Hemisphere), as observed by Mei and Pasquero (2013) and Jansen et al. (2010). However, both studies imply this shift is approximately 5–10 km day^{-1}; therefore, this impact is small during the period when the cyclone core is over the largest SSTAs.

As discussed earlier, previous work, primarily interested in intense TCs, found that entrainment mixing contributes to approximately 80% of SSTAs following TC passage (Price 1981; D'Asaro et al. 2007; Huang et al. 2009). Figure 7 shows the fractional contribution to the TC cold wake arising from the turbulent mixing parameterization component [second term in Eq. (2)] as a function of S–S TCs for both configurations. The other contributor to cooling is surface enthalpy fluxes [first term in Eq. (2)] such that the contributions from both components sum to 1. At low surface wind speeds (weak storms), the fractional values in Fig. 7 are small. For tropical storms, the turbulence term contributes to approximately 12% of cooling, implying that enthalpy extraction (88%) dominates cold wake processes. At higher wind speeds (category 1 and higher), this fraction rises substantially, indicating that the mixing or upwelling component in Eq. (2) contributes to 85%–95% of simulated SSTAs. These results are in good agreement with the modeling results in Vincent et al. (2012b), who found that the combination of turbulence and advective processes only contributed 28% of the surface cooling for weak cyclones, but 81%–91% for the strongest TCs. The simplified model outlined here not only correctly parameterizes the overall SST response to TCs, but also the partitioning of processes contributing

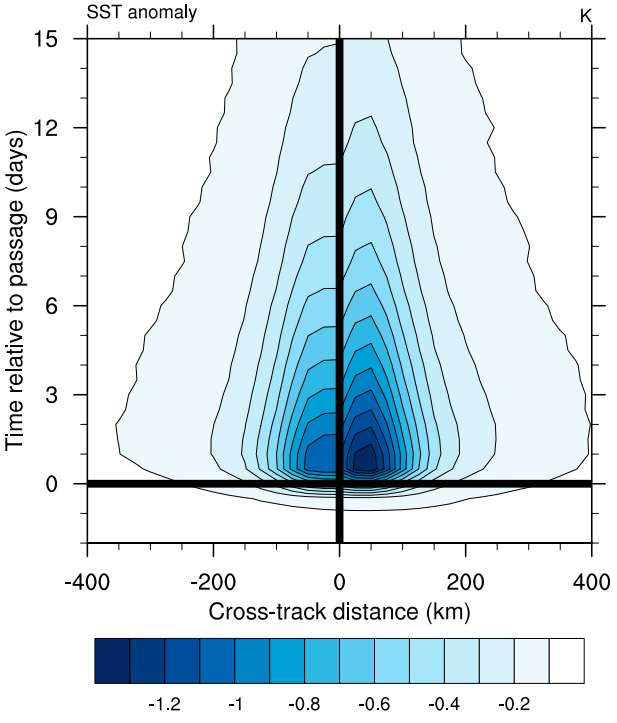

FIG. 6. Mean cross-track SSTA for TC passage as a function of time for the SLAB1 ensemble. Negative (positive) values along the *x* axis are locations to the left (right) of forward motion vector. Only storms of hurricane strength ($u_{10} > 33\,\mathrm{m\,s^{-1}}$) are used for compositing.

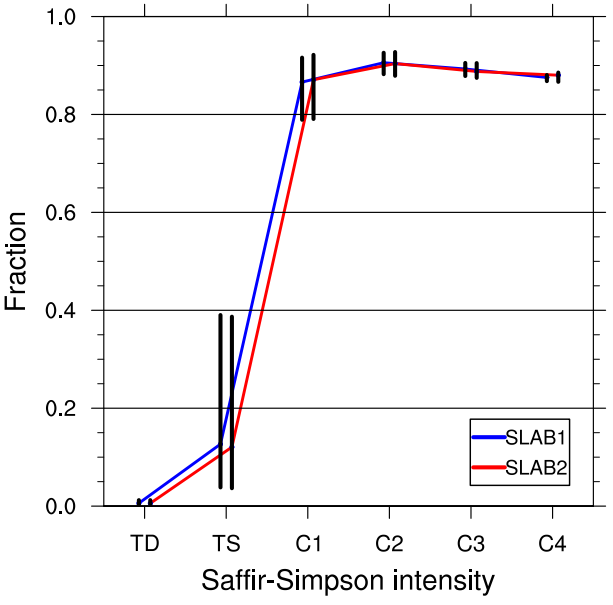

FIG. 7. Fraction of SST cooling arising from the turbulent mixing parameterization in Eq. (2) as a function of S–S storm intensity. All other cooling arises from surface enthalpy fluxes. Black bars denote the interquartile range of cooling. Cooling from both the SLAB1 and SLAB2 configuration functions are shown in blue and red, respectively.

to cold wakes. Compared to Vincent et al. (2012b), the amount of cooling for weak storms due to mixing is slightly too small here (by approximately 10%–15%), indicating that the parameterization is not active enough at low wind speeds (leaving too much of the cooling to be generated from enthalpy fluxes), although this impact is minimized by the relatively weak cold wakes for weak TCs (see Table 4). Interestingly, SLAB1 and SLAB2 performed quite similarly, even given different forcing functions as TC intensity increases. While this is certainly due in part to the definition of forcing function, it also may serve as support for the findings of Lloyd and Vecchi (2011), who hypothesize that SSTAs provide a regulation aspect to TC intensification.

4. Impact of cold wakes on TC climatology

Since it can been demonstrated that this setup produces highly similar TC samples (section 2c) and realistic TC cold wakes (section 3) without impacting the large-scale climatology of the simulations (shown in the appendix), intensity errors associated with prescribed SSTs are assessed. Table 5 shows the breakdown for all storms tracked in each configuration (FIXED, SLAB1, and SLAB2). The total number of storms is 5%–9% higher in the FIXED configuration relative to the configurations with interactive oceans. While this number is relatively small, it demonstrates that even marginal cooling under weak, incipient storms may be sufficient to decrease surface enthalpy fluxes enough to hinder genesis and intensification in climate models. The average duration for storms is also slightly shorter in both slab ocean configurations, further indicating that not accounting for SSTAs may allow TCs to persist longer than if this cooling is considered. Plots of track density (not shown) indicate, however, that these differences between configurations are comparably small regionally relative to existing climatological biases (relative to observations) in 0.25° resolution CAM5 simulations. In some instances, this overall reduction in count and lifetime helps alleviate biases in areas where too much TC activity occurs (eastern and central Pacific and eastern North Atlantic), but areas where CAM produces too little TC activity, such as the western Pacific and western Atlantic, see similar or slightly degraded spatial skill with both the SLAB1 and SLAB2 configurations (relative to FIXED). Further comparison of CAM TC climatology with observations can be found in Bacmeister et al. (2014), Zarzycki and Jablonowski (2014), Wehner et al. (2015), and Reed et al. (2015).

TABLE 5. Total number of storms in 25 years of simulations for each configuration. Also shown is the average storm lifetime as well as the number of storms reaching each Saffir–Simpson category.

	FIXED	SLAB1	SLAB2
No. of storms	1270	1189	1162
Avg lifetime (h)	175.3	168.3	163.8
Tropical storm	423	445	425
Category 1	319	340	344
Category 2	149	160	167
Category 3	209	183	166
Category 4	150	60	58
Category 5	20	1	2

Also shown in Table 5 is the number of TCs in each simulation that reaches a specific S–S category. The maximum intensity a TC reached at any 6-hourly point during its trajectory is binned. The number of tropical storms and weak hurricanes (categories 1 and 2) is actually larger in the simulations utilizing the slab ocean, even though, as discussed above, the total number of TCs is lower. This is offset by a large difference at higher intensities, with the FIXED configuration producing significantly more storms of categories 3–5 than either the SLAB1 or SLAB2 runs. The FIXED configuration produces approximately 3 times the total number of category 4 storms in either of the interactive ocean configurations. Even more striking, only three category 5 TCs are generated in both slab ocean configurations combined (over 50 years), whereas the prescribed SST simulations produce approximately one category

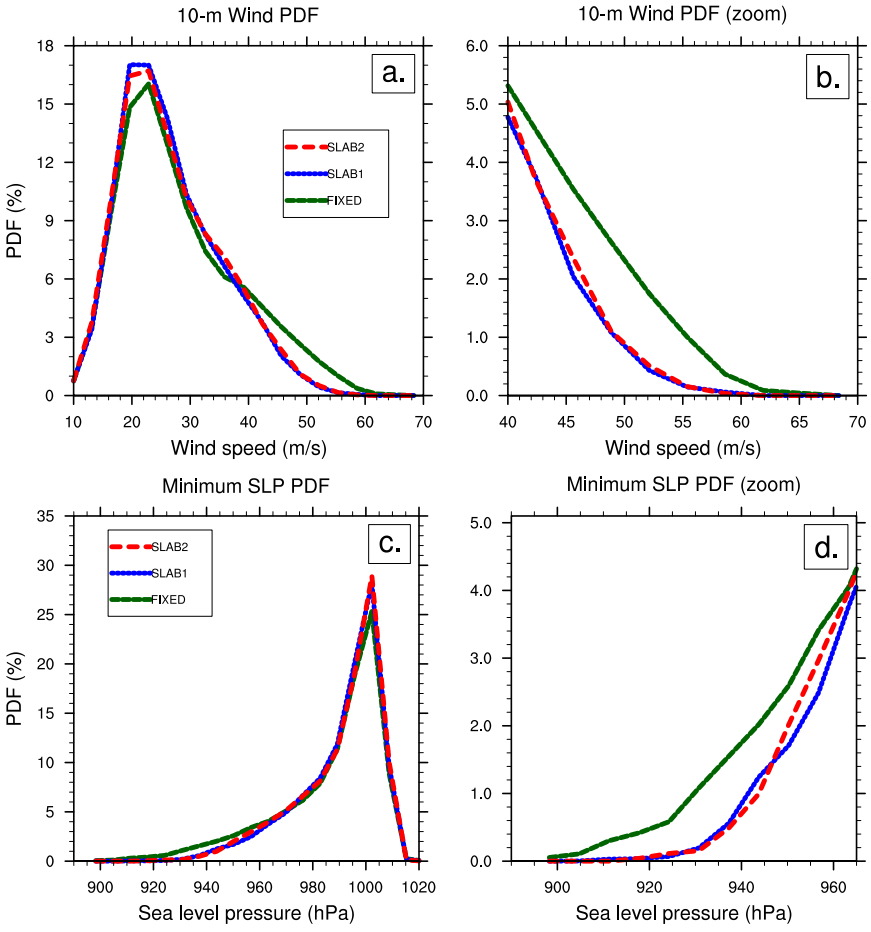

FIG. 8. Probability density function of all tracked TCs in each configuration: (a), (b) u_{10} (m s^{-1}) and (c),(d) SLP (hPa). (left) The entire distribution and (right) the distribution tail (most intense TCs) for each variable.

5 storm per year (a 90%–95% reduction when two-way coupling is implemented).

Figure 8 shows the frequency distribution of simulated 6-hourly intensities for all TCs tracked in the three experiments. All points along each TC trajectory are considered. The 10-m wind is shown in Figs. 8a,b, with minimum SLP shown in Figs. 8c,d. Figures 8b,d are zoomed in on the tails of the distribution (most intense storms). The majority of TCs in all simulations are relatively weak, with the most frequent intensity being approximately 20–25 m s^{-1} (tropical storm strength). For both SLP and wind, prescribed SSTs result in a longer tail (higher frequency of more intense storms). The shift between the FIXED configuration and either SLAB1 or SLAB2 is far larger than the difference between the slab configurations themselves, implying that the impact of the two different forcing functions is quite small, even for very intense TCs, when compared to the difference between an interactive and noninteractive ocean surface.

The Kolmogorov–Smirnov (KS) two-sample test can be applied to determine if the intensity distributions (samples) shown in Fig. 8 can be drawn from the same underlying nonparametric distribution (the null hypothesis) (Young 1977; Ferro et al. 2005). Using the KS test, the frequency shifts in the entire SLP and 10-m wind distributions for both SLAB1 and SLAB2 (compared to the control case, FIXED) are statistically significant at the 99.9% level. As expected, this conclusion holds true if only the tails of the distributions are subsampled (most intense 10%, 5%, and 1%). This not only confirms that the large ensemble sample provides a robust technique for isolating TC air–sea feedbacks in CAM, but it can be concluded with a very high degree of certainty that the choice of ocean treatment in these simulations impacts TC climatology in a significant manner.

Table 6 quantifies some of the results seen in Fig. 8. Over all 6-hourly points, the mean SLP (10-m wind) is increased (decreased) by approximately 3 hPa (1.5 m s^{-1})

TABLE 6. Intensity statistics for simulated tropical cyclones in each configuration. Statistics are drawn from entire pool of 6-hourly measurements during all 25 years of simulations for each configuration.

	FIXED	SLAB1	SLAB2
Mean SLP (hPa)	987	990	990
Low 5% SLP	943	957	957
Low 1% SLP	922	941	942
Low 0.1% SLP	902	924	925
Min SLP	887	908	916
Mean u_{10} ($m\,s^{-1}$)	28.2	26.6	26.7
High 5% wind	48.2	42.8	43.1
High 1% wind	55.0	49.1	49.2
High 0.1% wind	60.7	55.5	55.1
Max wind	66.5	59.8	60.0

TABLE 7. Mean integrated surface heat fluxes for all simulated TCs (top) and hurricanes only (>33 $m\,s^{-1}$; bottom) along with mean V_{pot}. Fluxes shown are latent (LHFLX) and sensible (SHFLX). Reduction in total (latent + sensible) flux $\Delta_{TOTFLUX}$ and ΔV_{pot} (relative to FIXED) is also shown for the SLAB1 and SLAB2 configurations. All values calculated using 1° grid box on TC center during exact time of passage (day 0).

	LHFLX ($W\,m^{-2}$)	SHFLX ($W\,m^{-2}$)	$\Delta_{TOTFLUX}$ (%)	V_{pot} ($m\,s^{-1}$)	ΔV_{pot} ($m\,s^{-1}$)
All TCs					
FIXED	299.6	63.1	—	67.8	—
SLAB1	246.0	48.6	−18.8	66.2	−1.9
SLAB2	246.8	48.9	−18.5	66.2	−2.4
Hurricanes only					
FIXED	506.9	118.8	—	68.8	—
SLAB1	382.3	83.9	−25.5	64.8	−5.2
SLAB2	376.0	82.3	−26.8	64.2	−5.5

by TC-induced SSTAs in both the SLAB1 or SLAB2 experiments relative to FIXED. This discrepancy becomes more prominent if only the strongest TCs are considered, with SLPs being 20 hPa stronger in the FIXED experiment for the most intense 1% of TC data points (~6 $m\,s^{-1}$ for 10-m winds). This intensity shift is further highlighted in even more restrictive quantities measuring the tail of the distribution (most intense 0.1% and overall most intense TC), although the intensity gap between the interactive and noninteractive cases does not materially increase with increasing storm strength.

In aggregate, SSTAs directly under the core of the TC (day 0) in the SLAB1 and SLAB2 configuration (relative to the FIXED climatological baseline) are −0.32 and −0.41 K, respectively, for all TCs (−0.80 and −0.87 K for storms ranked category 1 and higher). Recall that SSTAs are actually maximized 1–2 days after the center of the TC passes, which is why these values are less than those shown in Table 4. These results show that the shifts in the intensity distributions discussed above are the result of cooler SSTs under the core of the simulated storms and, therefore, reduced surface enthalpy fluxes driving TC thermodynamic processes. Using buoy observations, Cione and Uhlhorn (2003) found that total enthalpy fluxes within the core (radius of 60 km) of strong TCs were reduced by approximately 40% by SSTAs. CAM-modeled TC latent and sensible heat fluxes (using a 1° box on TC center) are shown in Table 7. For all TCs (Table 7, top), total enthalpy is reduced by 19% when using an interactive ocean surface, with the majority of the reduction arising from the decrease in latent heat. This overall response is similar to the results of Jullien et al. (2014), who used a coupled regional model over the South Pacific. If only hurricanes are isolated [Table 7, bottom, as in Cione and Uhlhorn (2003)], the addition of an interactive ocean (with realistic cold wakes) results in a larger enthalpy decrease of 26%–27% when compared to the fixed SST case.

Further, an estimate of maximum potential intensity V_{pot} ($m\,s^{-1}$) can be calculated using the formulation defined by DeMaria and Kaplan (1994):

$$V_{pot} = 28.2 + 55.8e^{0.1813(SST - SST_0)}, \quad (4)$$

where SST_0 is a reference temperature equal to 303.15 K. Within the same 1° box, the average under-TC SST can be used to calculated mean maximum potential intensities (MPIs), which are also shown in Table 7. Overall, V_{pot} is reduced from 67.8 $m\,s^{-1}$ (prescribed SSTs) to 66.2 $m\,s^{-1}$ for both SLAB1 and SLAB2. When only considering hurricane-strength TCs, this reduction in MPI is more striking, being reduced by 5.2 and 5.5 $m\,s^{-1}$ for SLAB1 and SLAB2, respectively. The latter reduction, in particular, agrees well with wind speed reductions in the tail of the intensity distribution (Fig. 8 and Table 6) when SST cooling is allowed.

As a converse experiment, the SLAB1 model is run offline using forcing from the FIXED case. Therefore, the ocean surface is allowed to change in a dynamic manner; however, the model is only coupled in one direction, with the modified SSTs providing no feedback to the atmosphere, allowing for the lack of regulation to be addressed in an indirect sense. Figure 9a shows the reduction in SLP as a function of both ambient background SST and SSTA. This is calculated by binning TCs from the online SLAB1 and offline SLAB1 (forced with FIXED atmosphere) by both ambient SST and SSTA (1° footprint at +1 day following TC passage), taking the average storm intensity in each bin for each configuration, then subtracting the two. Reduction in TC intensity is maximized for a combination of warm ambient SSTs (28°–30°C) and large

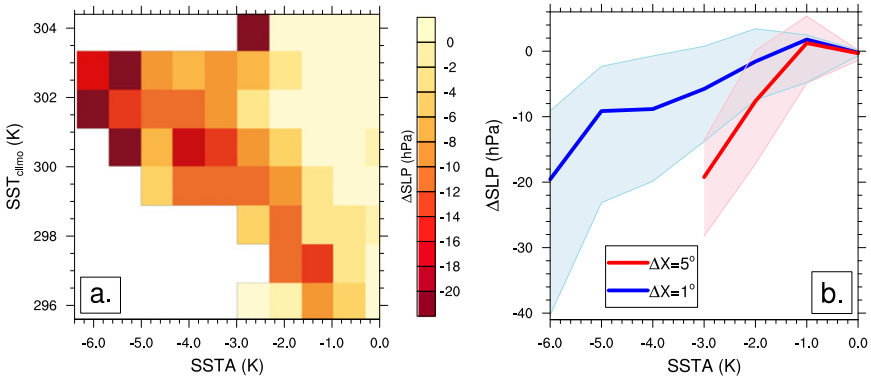

FIG. 9. Reduction in sea level pressure associated with two-way coupling vs one-way coupling. (a) Reduction in SLP ΔSLP as a function of both ambient (background) SST and SSTA, and (b) mean ΔSLP for all ambient SSTs as a function of SSTA. SSTA is measured one day following TC passage by averaging over a 1° grid box in (a) and both 1° and 5° grid boxes in (b). Shading represents 5% and 95% percentiles in (b).

amounts of cooling (4°–6°C), which is reasonable given that larger cold wakes (and therefore negative feedbacks) are induced by stronger surface winds. Strong storms that form in warm SST conditions in the FIXED case would theoretically generate these strong cold wakes, but the lack of under-TC cooling due to the noninteractive ocean surface allows for storm intensification and maintenance to be unregulated by this feedback.

By averaging across ambient SSTs, Fig. 9b shows the average reduction in storm intensity per degree SSTA. The blue (red) curve shows the relationship if the SSTA is defined over a 1° (5°) grid box. Note that, while the mean maximum reduction in SLP is essentially similar (20 hPa), the SSTA associated with that reduction differs by approximately a factor of 2, depending on how the SSTA is defined spatially. These results imply an approximate mean decrease in TC intensity of between 3 and 7 hPa K^{-1} cooling. This is slightly lower than estimates from theoretical studies (e.g., Emanuel 1986; Holland 1997) but in line with previous simplified or limited-area modeling assessments (Schade and Emanuel 1999; Bender and Ginis 2000; Jullien et al. 2014). It is worth noting that the manner in which SSTA is calculated varies widely across published literature investigating this feedback, so, as shown in Fig. 9b, there remains a large degree of uncertainty if this lack of standardization is unaccounted for.

The impact of SST cooling on physical TC structure is displayed in Fig. 10. Shown in Fig. 10 are averaged composite panels for the 15 strongest simulated TCs at their peak intensity in each configuration: 850-hPa horizontal wind (WIND850; Figs. 10a–c), outgoing longwave radiation (FLUT; Figs. 10d–f), and instantaneous precipitation rate (PRECT; Figs. 10g–i) are plotted. Composites are taken over a 6° × 6° box, with the center of each TC being defined by minimum SLP location.

For all three variables, the FIXED case (Figs. 10a,d,g) produces a more intense composite TC than either SLAB1 (Figs. 10b,e,h) or SLAB2 (Figs. 10c,f,i). The 850-hPa winds (Figs. 10a–c) are clearly stronger, with 70 m s^{-1} winds wrapping completely around the storm's eye, which is not the case with either slab configuration. Additionally, the spatial extent of the wind field is larger in the FIXED case. This size comparison is also evident in the outgoing longwave radiation panels (Figs. 10d–f). While the lowest values (an approximation of cold cloud-top temperature) are roughly the same between all three configurations, the size of the 120 W m^{-2} contour is largest in the FIXED case, indicating a larger central dense overcast. The eye is also warmer (higher FLUT) and most distinct for FIXED when compared to SLAB1 or SLAB2. The same conclusions are seen in the precipitation panels (Figs. 10g–i), where the FIXED simulations produce cyclones with more extreme rainfall rates in the core as well as an increased spatial extent of the 20 and 0.5 mm h^{-1} contours.

While SST cooling underneath the core of the TC is the primary driver of this decrease in high-end intensity as simulated in CAM, one other such mechanism may be the phenomenon of "cold wake crossing." In this case, another cyclone may pass over the lingering cold wake of a TC that induced an SSTA a few days to weeks prior to the second storm's passage (Brand 1971). Balaguru et al. (2014) found that approximately 7.5%–15.4% of TCs in the northern Atlantic and Pacific Ocean basins may interact with a previously existing cold wake. If a −0.5-K SSTA existing three days prior to TC passage defines a preexisting cold wake, 11.8% and 16.6% of all SLAB1 and SLAB2 TCs interact with a previous cyclone through this mechanism. Given the agreement with Balaguru et al. (2014) with this occurrence frequency, it

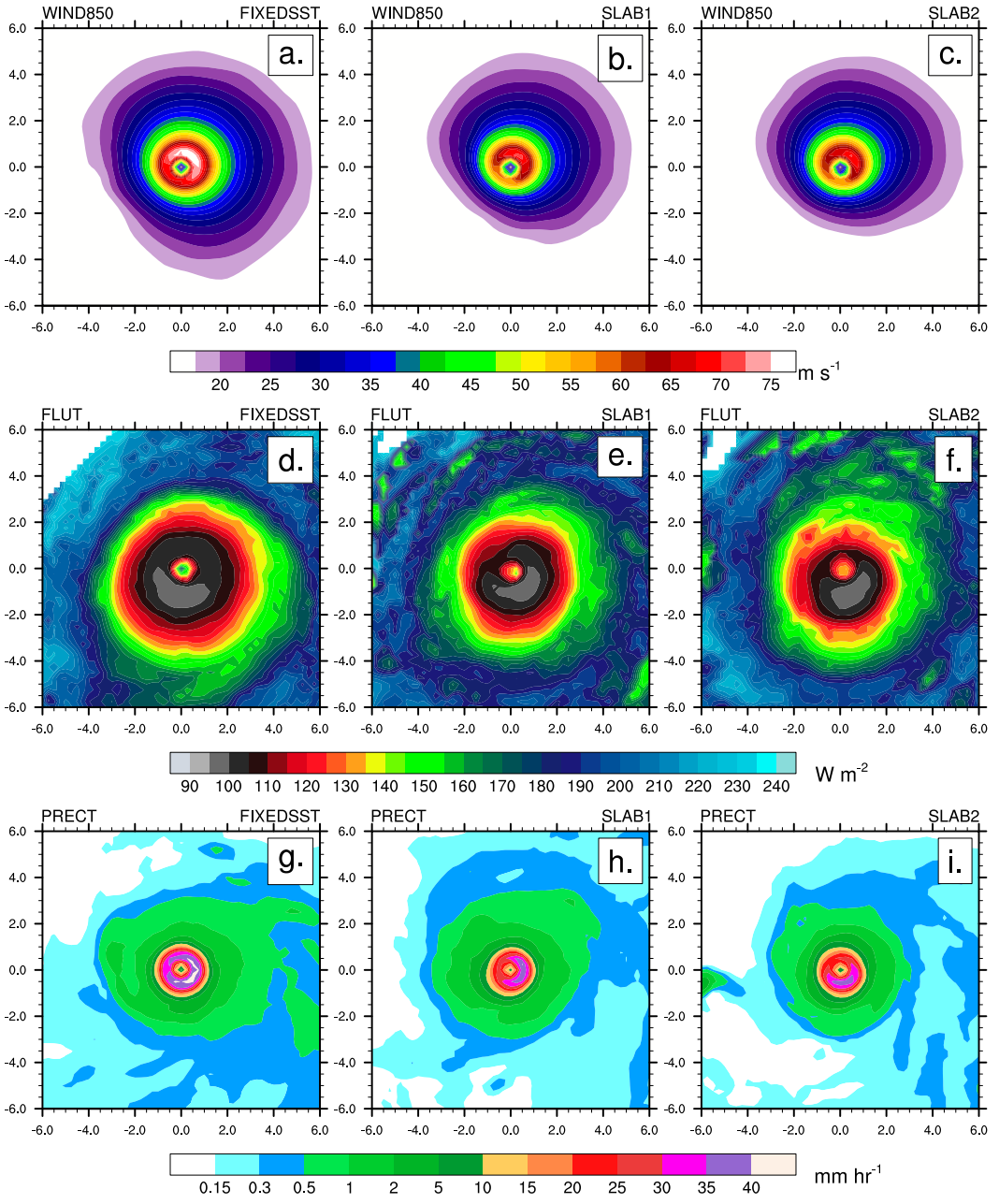

FIG. 10. Composite plots of instantaneous horizontal structure of the 15 strongest TCs at peak intensity in (left) FIXED, (center) SLAB1, and (right) SLAB2 ensemble configurations. Variables shown are (a)–(c) 850-hPa horizontal wind, (d)–(f) outgoing longwave radiation, and (g)–(i) instantaneous precipitation rate. Storms are composited by averaging over a common domain, with each TC center defined by its SLP minimum.

seems plausible that their findings of suppressed intensification rates associated with TC–TC cold wake interaction are applicable in this study as well. Furthermore, while nondeveloping TCs are not addressed here, this cold wake interaction represents another process that may result in decreased storm count within the slab ocean configurations, as seen in Table 5, since a fraction of pregenesis features likely encounter existing cold wakes, thereby decreasing surface energy available to allow them to intensify into a TC.

5. Sensitivity simulations

Although past work indicates that thermodynamic fluxes alone cannot account for observed cooling under strong TCs (Vincent et al. 2012b), 10 simulations

(compared to 25 in the control cases) are performed with a traditional slab ocean. These simulations are identical to the SLAB1 and SLAB2 configurations, but the middle (mixing) term in Eq. (2) is set to 0. The resulting mean SSTAs from the traditional slab ocean [thermodynamic only (THERMO)] are compared to the control runs and Mei and Pasquero (2013, hereafter MP13) in Table 8. MP13 is chosen as an observational comparison since their results represented the most recent study cited here.

As expected, cold wakes are generated in THERMO, even without parameterized mixing, since large quantities of sensible and latent heat are still removed from the ocean surface by TCs. However, while cooling increases as a function of storm strength, the overall SSTA magnitudes, particularly for intense storms (e.g., categories 3–5), are much smaller than either the SLAB1 or SLAB2 configurations or observations. Also shown in Table 8, these smaller SSTAs result in far less of a reduction in storm intensity, with the decrease in SLP being only a few hectopascals when compared to the FIXED runs. This confirms that thermodynamic-only slab oceans cannot adequately represent cold wakes and their feedbacks without the additional parameterization of turbulent mixing.

Because of the large spread in estimates of cold wake magnitudes in published literature (see Table 4), it is also prudent to perform a few rudimentary sensitivity studies to verify that intensity reductions found here are robust for a range of simulated SST cooling close to observations. Five extra sets of simulations of SLAB1 (10 members each) are performed. The first three sets test sensitivity to parameterized cooling rate R_{cool}, whereas the final two sets assess modifications to the relaxation (*e*-folding) time scale τ over which SSTs recover to climatological values. SLAB2 is not assessed because of the high degree of similarity with SLAB1 in the control simulations.

Since R_{cool} exerts a strong force on overall SST cooling, it is expected that varying this parameter may have a large impact on simulated cold wakes and corresponding intensity shifts. Table 9 shows that, as R_{cool} is increased, cooling increases across all intensity classes. With respect to MP13's estimates, an R_{cool} of 11.75 K day^{-1} produces more closely matched SSTAs for all classifications (when compared to the control configuration, R_{cool} = 4.7 K day^{-1}), with only slight overcooling for TCs category 3 or stronger (1.56 vs 1.45 K).

This additional cooling shows the negative feedback discussed in section 4 may be even larger. For example, the strongest 5% and 1% of TCs were an additional 4 hPa weaker by SLP (2.5 m s^{-1} by 10-m wind, not shown) when the R_{cool} = 11.75 K day^{-1} case is compared to the control SLAB1. The strongest storm generated in the same simulation was significantly weaker than the maxima attained in any of the other simulations, with a minimum SLP of 924 hPa. Similar behavior is shown for the less extreme modifications of R_{cool}, with a smaller increase (and small decrease) in R_{cool} resulting in slightly weaker (stronger) TCs when compared to the control SLAB1 simulations due to larger (smaller) SSTA magnitudes.

When adjusting for the recovery time scale of SSTs following TC passage, less sensitivity is observed. Table 10 shows that marginal additional SST cooling was found with larger τ values, indicative of slightly weaker relaxation forcing during SST recovery during and following TC passage. However, this difference was only approximately 0.06 K between τ = 5 days and τ = 10 days for the strongest storms and only 0.02 K for all storms. These small differences in SST do not have dramatic impacts on storm intensity, with SLP showing no clear signal either for the mean of all generated TCs or in the tail of the distribution (Table 10).

TABLE 8. SSTA and SLP intensity statistics when using a THERMO slab ocean compared to results in FIXED, SLAB1, and SLAB2 runs. MP13 are used as an observational reference. All SSTAs are calculated over a 5° × 5° footprint for direct comparison to MP13 and are broken down by various Saffir–Simpson categories. For SLP, the mean value for all tracked TCs is reported, along with the threshold for most intense 5% and 1% of storms as well as the maximum intensity attained amongst all ensemble members. Configurations denoted with an asterisk are composed of 10 ensemble members; all others are composed of 25.

	MP13	FIXED	SLAB1	SLAB2	THERMO*
SSTA (K)					
TD	−0.38	—	−0.11	−0.16	−0.10
TS	−0.71	—	−0.18	−0.28	−0.14
C1–C2	−1.17	—	−0.61	−0.76	−0.24
C3–C5	−1.45	—	−1.01	−1.11	−0.24
C1–C5	−1.27	—	−0.63	−0.78	−0.24
AS	−0.72	—	−0.29	−0.40	−0.16
SLP (hPa)					
Mean	—	987	990	990	988
5%	—	943	957	955	946
1%	—	922	941	939	922
Max	—	887	908	904	894

6. Discussion and conclusions

This paper describes an idealized, empirically based, inexpensive slab ocean that approximates SST cooling resulting from both flux extraction and turbulent mixing and upwelling associated with the passage of tropical cyclones. The parameterization is designed to produce cold wakes highly similar to published observations while maintaining a prescribed large-scale background SST climatology, allowing for direct and isolated comparison with simulations using one-way coupled SSTs. Cold wakes produced by this configuration are realistic in magnitude, spatial structure, and temporal extent when

TABLE 9. As in Table 8, but showing sensitivity of SSTA and SLP intensity statistics to varying values of R_{cool} (K day^{-1}) in Eq. (2) for the SLAB1 configuration.

	MP13	FIXED	R_{cool} = 2.35*	R_{cool} = 4.7	R_{cool} = 7.35*	R_{cool} = 11.75*
SSTA (K)						
TD	−0.38	—	−0.11	−0.11	−0.12	−0.14
TS	−0.71	—	−0.16	−0.18	−0.21	−0.25
C1–C2	−1.17	—	−0.38	−0.61	−0.74	−1.03
C3–C5	−1.45	—	−0.78	−1.01	−1.22	−1.56
C1–C5	−1.27	—	−0.40	−0.63	−0.75	−1.04
AS	−0.72	—	−0.22	−0.29	−0.34	−0.43
SLP (hPa)						
Mean	—	987	990	990	990	991
5%	—	943	956	957	958	961
1%	—	922	935	941	944	946
Max	—	887	904	908	909	924

compared to observational and other modeling studies. This framework produces nonnegligible cooling directly under the core of the cyclone and a peak SSTA 1–2 days following the passage of a TC center. A simple thermodynamic-only slab ocean cannot correctly simulate these features, highlighting the necessity of a representation of mixing to properly approximate cold wakes.

TCs produced by interactive ocean configurations are universally weaker because of reduced surface enthalpy fluxes. This is particularly noticeable for the most intense storms, where surface wind (sea level pressure) intensities may be decreased by more than 5 m s^{-1} (20–30 hPa) when compared to prescribed SST experiments. This decrease in intensity is consistent with thermodynamic theory, with the majority of air–sea enthalpy decreases resulting from a reduction in latent heat from a cooler ocean surface. The estimated decrease in intensity per kelvin cooling roughly agrees with previous numerical modeling studies using coupled limited-area or otherwise idealized setups, although the lack of standardization in the definition of cold wake magnitude (both in time relative to TC passage and spatial averaging) makes direct comparison difficult. The overall number of TCs generated, as well as their lifetimes, is also reduced, likely due to both reductions in SSTs under incipient vortices and situations where a TC may come upon an SSTA induced by a previous storm.

Since TC impacts such as wind damage, flooding, and storm surge are disproportionately associated with the most intense storms (Goldenberg et al. 2001; Blake et al. 2011; Needham et al. 2015), the results here imply that caution is required when interpreting individual events simulated in high-resolution climate experiments with prescribed SSTs. For example, using distinct S–S categories, simulations with noninteractive SSTs lead to 3 times more category 4 and 10–20 times more category 5 hurricanes annually in the Northern Hemisphere when compared to two-way coupled simulations. Given that this feedback is also demonstrated to be nonlinear with respect to both storm intensity and underlying SSTs; this may be particularly problematic for studies attempting to simulate and quantify trends in intensity in a discrete sense (e.g., the number of landfalling category 3 and higher TCs in a future climate).

Drawbacks exist with respect to using such a highly idealized and simplistic scheme. The most obvious one is perhaps the use of a fixed mixed layer depth in time. In reality, turbulent mixing induces a deepening of the mixed layer, which may persist for many weeks. These impacts have been hypothesized to drive climate system ''memory'' of TC passages and may either decrease the suitability of a region to maintain TCs (e.g., cooler surface waters) or precondition the ocean to act as a larger integrated heat source (e.g., warmer waters being mixed downward and rapid SSTA recovery providing more integrated heat content; Hart et al. 2007). Additionally, as a column-based method, the ability for a cold wake to

TABLE 10. As in Table 8, but showing sensitivity of SSTA and SLP intensity statistics to varying values of τ (days) in Eq. (2) for the SLAB1 configuration.

	MP13	FIXED	τ = 5*	τ = 8	τ = 10*
SSTA (K)					
TD	−0.38	—	−0.09	−0.11	−0.10
TS	−0.71	—	−0.17	−0.18	−0.19
C1–C2	−1.17	—	−0.58	−0.61	−0.64
C3–C5	−1.45	—	−1.01	−1.01	−1.12
C1–C5	−1.27	—	−0.60	−0.63	−0.66
AS	−0.72	—	−0.28	−0.29	−0.30
SLP (hPa)					
Mean	—	987	989	990	990
5%	—	943	954	957	955
1%	—	922	938	941	939
Max	—	887	919	908	904

have an impact on the surrounding ocean waters in the horizontal direction is neglected (either via horizontal mixing, conduction, or inertial effects). This includes variations in oceanic meridional heat transport as proposed by Sriver and Huber (2007). The use of a mean state also overlooks the ability of transient cyclonic (anticyclonic) ocean eddies to enhance (inhibit) SSTA feedbacks (Bao et al. 2000). However, adding the aforementioned complexity should not impact the core findings here regarding intensity biases in a long-term, mean, climatological sense.

The frequency of modeling groups investigating TC behavior in high-resolution (0.5° or finer) fully coupled simulations has increased in the last few years. As discussed earlier, Small et al. (2014) was able to generate TCs in a 0.25° resolution coupled experiment, albeit with climatological deficiencies due to ocean biases. Kim et al. (2014) used the GFDL CM2.5 at 50-km (25 km) atmospheric (oceanic) resolution and found that, like Small et al. (2014), cold SST biases (as well as subsidence and wind shear that were larger than observations) resulted in too few TCs being simulated in the North Atlantic. Newer simulations, utilizing the GFDL High-Resolution Forecast-Oriented Low Ocean Resolution (HiFLOR) coupled model, show partially improved biases in the North Atlantic but an overestimation of TCs in the western and central Pacific basins (Murakami et al. 2015). Vecchi et al. (2014) and Ogata et al. (2016) have demonstrated some degree of improvement in TC activity in lower-resolution atmosphere–ocean models by applying a flux correction technique to reduce SST biases, which may be a promising strategy to improve coupled simulations in the future. It should be expected that more of these simulations will come online in the coming years as available computing resources continue to increase, providing more data points for consideration.

Coupling high-resolution simulations to three-dimensional prognostic ocean models is the gold standard of future earth system modeling initiatives. However, existing long-term climatological biases in these ocean models also need to be addressed so as to provide the correct large-scale surface characteristics required for adequately simulating the spatial climatology and seasonal cycle of TC activity. The recommendation implicit in these results is that global models capable of producing realistic TC intensities should strongly consider the addition of a simplified ocean parameterization in lieu of one-way coupled prescribed SSTs in order to produce more physically consistent TC results if computational constraints or model biases make fully coupled runs impractical. Future work will further explore the hierarchy of ocean model complexity (e.g., multilayer mixed layer models) in pursuit of this goal.

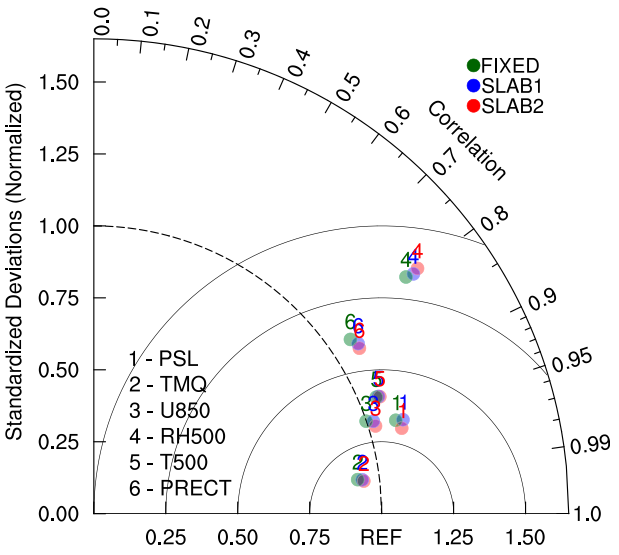

FIG. A1. Taylor diagram of mean climate statistics for all ensemble members for each model configuration.

Acknowledgments. NCAR's Advanced Study Program (ASP) postdoctoral research fellowship provided funding for this work. CMZ would like to thank Brian Medeiros and Justin Small for providing feedback that improved this manuscript. High-performance computing support from Yellowstone (http://n2t.net/ark:/85065/d7wd3xhc) was utilized to complete the simulations shown here and was provided by NCAR's Computational and Information Systems Laboratory, sponsored by the National Science Foundation.

APPENDIX

Comparison of Large-Scale Climatology

To demonstrate that the mean climatology (and therefore the large-scale forcing) is the same between the simulations, Taylor statistics for the three configurations (all ensemble members) are shown in Fig. A1. Statistics are calculated over the June–November (inclusive) period from 0° to 60°N and from 115° to 5°W (roughly the area of the high-resolution domain). The absolute distance of a point from the origin (bottom left of Fig. A1) denotes the magnitude of the variability within the domain (normalized standard deviation), whereas the spatial pattern correlation is plotted as the radial angle between a model marker and the origin. A comprehensive discussion of this form of analysis can be found in Taylor (2001). Green dots demonstrate the climatology of the FIXED simulation, and blue and red dots mark results from the SLAB1 and SLAB2 configurations, respectively. Variables shown include sea level pressure (PSL

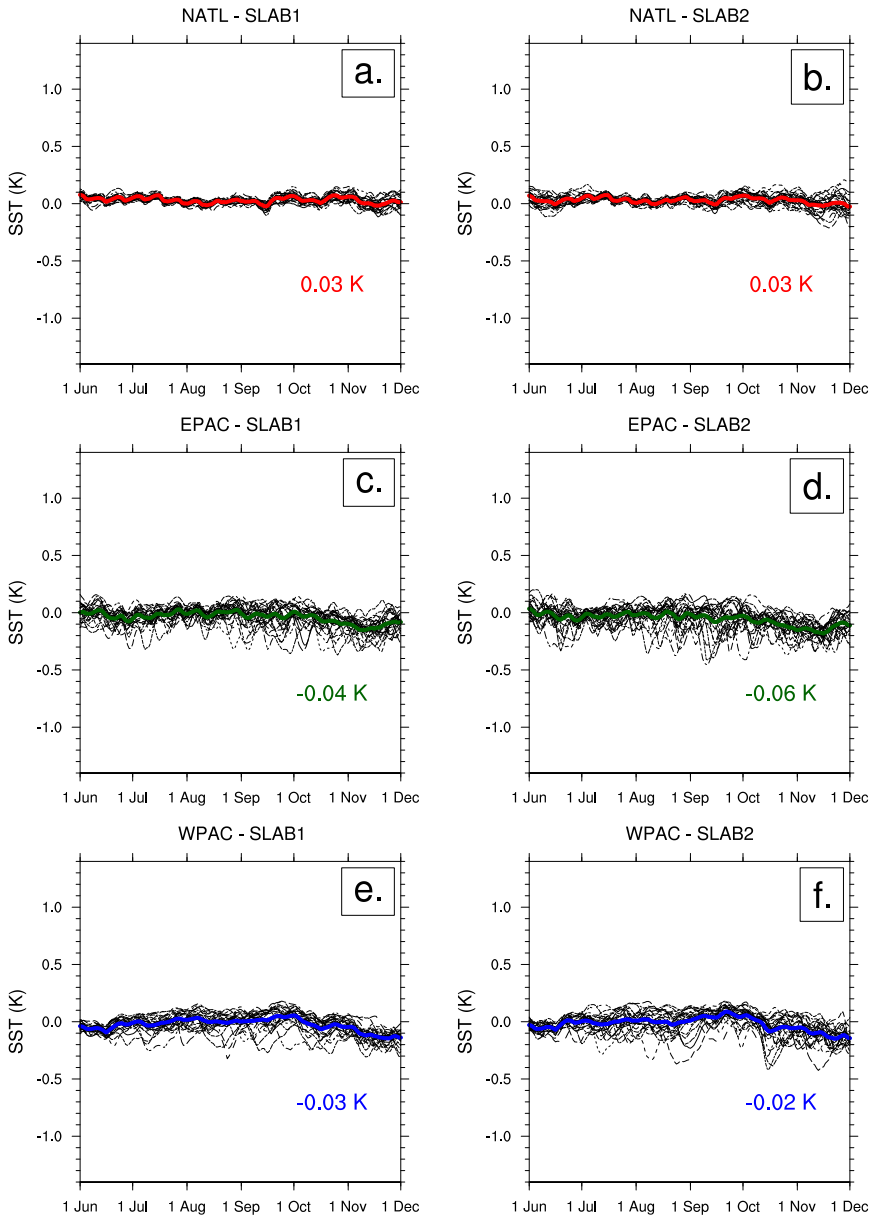

FIG. A2. Area-mean SSTA (SST deviation from FIXED climatology) as a function of time for (left) SLAB1 configuration and (right) SLAB2 configuration for the (a),(b) NATL (red), (c),(d) EPAC (green), and (e),(f) WPAC (blue). Each black line represents a separate ensemble member, with the mean denoted by a thick colored line. The June–November average SSTA for each ocean basin is also presented in each panel.

in Fig. A1), total precipitable water (TMQ), 850-hPa zonal wind (U850), 500-hPa relative humidity (RH500), 500-hPa temperature (T500), and total precipitation rate (PRECT in Fig. A1). The simulations are compared to reanalysis and observational datasets, including PSL, U850, RH500, and T500 from NCEP–NCAR reanalysis (Kalnay et al. 1996), TMQ from MERRA (Rienecker et al. 2011), and PRECT from TRMM (Huffman et al. 2007).

It is clear that each variable's points are tightly clustered for the three setups, indicating that the climatology for each variable is highly similar when the three configurations are compared. This provides strong evidence that the simulations using the slab ocean produce a near-identical mean state, and, therefore, the slab ocean implementation is not impacting the background large-scale climatology in the atmospheric component of the model. Since this analysis is only concerned with measuring the

relative difference between model configurations used in this study, readers are referred to Bacmeister et al. (2014) for a more thorough discussion of CAM5 skill (relative to observations) at high resolutions.

To confirm this, daily mean SSTAs, averaged over each ocean basin's main development region (MDR) for each ensemble member (thin black lines), are shown in Fig. A2. Basin-mean time series (all ensemble members) are shown as a thick colored curve (red in the North Atlantic, green in the eastern Pacific, and blue in the western Pacific). The seasonal mean SSTA is also calculated and shown in each panel. The MDRs are defined as the area from 10° to 20°N and from 80° to 20°W in the North Atlantic (Goldenberg and Shapiro 1996), 10°–20°N and 130°–95°W in the eastern Pacific, and 10°–25°N and 120°–170°E in the western Pacific (Pun et al. 2013). The FIXED configuration is not shown since it, by definition, forms the basis for the anomaly calculation (i.e., FIXED has a perpetual anomaly equal to 0 for all ensemble members).

As implied by the Taylor diagrams, SST drift (from climatology) is minimal, with average basin SST being constrained to less than 0.25 K for any particular ensemble member on any given simulation day. Mean seasonal SST biases for each basin are within 0.03 K of climatology for the North Atlantic (NATL) and western Pacific (WPAC) basins, where the most intense TCs are generated (see Fig. 3). Slightly larger biases exist in the eastern Pacific (EPAC) partly because of the smaller averaging region for the MDR, but also because of late-season SST cooling associated with strong mountain gap surface winds extending into the Gulf of Tehuantepec that become pronounced toward the end of boreal autumn (Chelton et al. 2000).

REFERENCES

Archambault, H. M., L. F. Bosart, D. Keyser, and J. M. Cordeira, 2013: A climatological analysis of the extratropical flow response to recurving western North Pacific tropical cyclones. *Mon. Wea. Rev.*, **141**, 2325–2346, doi:10.1175/MWR-D-12-00257.1.

Bacmeister, J. T., M. F. Wehner, R. B. Neale, A. Gettelman, C. Hannay, P. H. Lauritzen, J. M. Caron, and J. E. Truesdale, 2014: Exploratory high-resolution climate simulations using the Community Atmosphere Model (CAM). *J. Climate*, **27**, 3073–3099, doi:10.1175/JCLI-D-13-00387.1.

Balaguru, K., S. Taraphdar, L. R. Leung, G. R. Foltz, and J. A. Knaff, 2014: Cyclone–cyclone interactions through the ocean pathway. *Geophys. Res. Lett.*, **41**, 6855–6862, doi:10.1002/2014GL061489.

Bao, J.-W., J. M. Wilczak, J.-K. Choi, and L. H. Kantha, 2000: Numerical simulations of air–sea interaction under high wind conditions using a coupled model: A study of hurricane development. *Mon. Wea. Rev.*, **128**, 2190–2210, doi:10.1175/1520-0493(2000)128<2190:NSOASI>2.0.CO;2.

Barnett, T. P., and M. E. Schlesinger, 1987: Detecting changes in global climate induced by greenhouse gases. *J. Geophys. Res.*, **92**, 14 772–14 780, doi:10.1029/JD092iD12p14772.

Bell, R., J. Strachan, P. L. Vidale, K. Hodges, and M. Roberts, 2013: Response of tropical cyclones to idealized climate change experiments in a global high-resolution coupled general circulation model. *J. Climate*, **26**, 7966–7980, doi:10.1175/JCLI-D-12-00749.1.

Bender, M. A., and I. Ginis, 2000: Real-case simulations of hurricane–ocean interaction using a high-resolution coupled model: Effects on hurricane intensity. *Mon. Wea. Rev.*, **128**, 917–946, doi:10.1175/1520-0493(2000)128<0917:RCSOHO>2.0.CO;2.

——, ——, and Y. Kurihara, 1993: Numerical simulations of tropical cyclone–ocean interaction with a high-resolution coupled model. *J. Geophys. Res.*, **98**, 23 245–23 263, doi:10.1029/93JD02370.

Bengtsson, L., K. I. Hodges, and M. Esch, 2007: Tropical cyclones in a T159 resolution global climate model: Comparison with observations and re-analyses. *Tellus*, **59A**, 396–416, doi:10.1111/j.1600-0870.2007.00236.x.

Bitz, C. M., K. M. Shell, P. R. Gent, D. A. Bailey, G. Danabasoglu, K. C. Armour, M. M. Holland, and J. T. Kiehl, 2012: Climate sensitivity of the Community Climate System Model, version 4. *J. Climate*, **25**, 3053–3070, doi:10.1175/JCLI-D-11-00290.1.

Blake, E. S., C. Landsea, and E. J. Gibney, 2011: The deadliest, costliest, and most intense United States tropical cyclones from 1851 to 2010 (and other frequently requested hurricane facts). NOAA Tech. Memo. NWS NHC-6, 49 pp. [Available online at http://www.nhc.noaa.gov/pdf/nws-nhc-6.pdf.]

Brand, S., 1971: The effects on a tropical cyclone of cooler surface waters due to upwelling and mixing produced by a prior tropical cyclone. *J. Appl. Meteor.*, **10**, 865–874, doi:10.1175/1520-0450(1971)010<0865:TEOATC>2.0.CO;2.

Caron, L.-P., and C. Jones, 2012: Understanding and simulating the link between African easterly waves and Atlantic tropical cyclones using a regional climate model: The role of domain size and lateral boundary conditions. *Climate Dyn.*, **39**, 113–135, doi:10.1007/s00382-011-1160-8.

Chauvin, F., J.-F. Royer, and M. Déqué, 2006: Response of hurricane-type vortices to global warming as simulated by ARPEGE-Climat at high resolution. *Climate Dyn.*, **27**, 377–399, doi:10.1007/s00382-006-0135-7.

Chelton, D. B., M. H. Freilich, and S. K. Esbensen, 2000: Satellite observations of the wind jets off the Pacific coast of Central America. Part I: Case studies and statistical characteristics. *Mon. Wea. Rev.*, **128**, 1993–2018, doi:10.1175/1520-0493(2000)128<1993:SOOTWJ>2.0.CO;2.

Cione, J. J., and E. W. Uhlhorn, 2003: Sea surface temperature variability in hurricanes: Implications with respect to intensity change. *Mon. Wea. Rev.*, **131**, 1783–1796, doi:10.1175//2562.1.

Daloz, A. S., F. Chauvin, and F. Roux, 2012a: Impact of the configuration of stretching and ocean–atmosphere coupling on tropical cyclone activity in the variable-resolution GCM ARPEGE. *Climate Dyn.*, **39**, 2343–2359, doi:10.1007/s00382-012-1561-3.

——, ——, K. Walsh, S. Lavender, D. Abbs, and F. Roux, 2012b: The ability of general circulation models to simulate tropical cyclones and their precursors over the North Atlantic main development region. *Climate Dyn.*, **39**, 1559–1576, doi:10.1007/s00382-012-1290-7.

Dare, R. A., and J. L. McBride, 2011: Sea surface temperature response to tropical cyclones. *Mon. Wea. Rev.*, **139**, 3798–3808, doi:10.1175/MWR-D-10-05019.1.

D'Asaro, E. A., T. B. Sanford, P. P. Niiler, and E. J. Terrill, 2007: Cold wake of Hurricane Frances. *Geophys. Res. Lett.*, **34**, doi:10.1029/2007GL030160.

DeMaria, M., and J. Kaplan, 1994: Sea surface temperature and the maximum intensity of Atlantic tropical cyclones.

J. Climate, **7**, 1324–1334, doi:10.1175/1520-0442(1994)007<1324:SSTATM>2.0.CO;2.

Dennis, J. M., and Coauthors, 2012: CAM-SE: A scalable spectral element dynamical core for the Community Atmosphere Model. *Int. J. High Perform. Comput. Appl.*, **26**, 74–89, doi:10.1177/1094342011428142.

Donelan, M. A., B. K. Haus, N. Reul, W. J. Plant, M. Stiassnie, H. C. Graber, O. B. Brown, and E. S. Saltzman, 2004: On the limiting aerodynamic roughness of the ocean in very strong winds. *Geophys. Res. Lett.*, **31**, L18306, doi:10.1029/2004GL019460.

Donnadieu, Y., R. Pierrehumbert, R. Jacob, and F. Fluteau, 2006: Modelling the primary control of paleogeography on Cretaceous climate. *Earth Planet. Sci. Lett.*, **248**, 426–437, doi:10.1016/j.epsl.2006.06.007.

Emanuel, K., 1986: An air–sea interaction theory for tropical cyclones. Part I: Steady-state maintenance. *J. Atmos. Sci.*, **43**, 585–605, doi:10.1175/1520-0469(1986)043<0585:AASITF>2.0.CO;2.

——, 2015: Effect of upper-ocean evolution on projected trends in tropical cyclone activity. *J. Climate*, **28**, 8165–8170, doi:10.1175/JCLI-D-15-0401.1.

Evans, J. L., 1993: Sensitivity of tropical cyclone intensity to sea surface temperature. *J. Climate*, **6**, 1133–1140, doi:10.1175/1520-0442(1993)006<1133:SOTCIT>2.0.CO;2.

Evans, K. J., P. H. Lauritzen, S. K. Mishra, R. B. Neale, M. A. Taylor, and J. J. Tribbia, 2013: AMIP simulation with the CAM4 spectral element dynamical core. *J. Climate*, **26**, 689–709, doi:10.1175/JCLI-D-11-00448.1.

Ferro, C. A. T., A. Hannachi, and D. B. Stephenson, 2005: Simple nonparametric techniques for exploring changing probability distributions of weather. *J. Climate*, **18**, 4344–4354, doi:10.1175/JCLI3518.1.

Galvin, J., 2008: The weather and climate of the tropics: Part 7—Tropical revolving storms. *Weather*, **63**, 327–333, doi:10.1002/wea.252.

Ginis, I., 2002: Tropical cyclone–ocean interactions. *Adv. Fluid Mech.*, **33**, 83–114, doi:10.1002/wea.252.

Goldenberg, S. B., and L. J. Shapiro, 1996: Physical mechanisms for the association of El Niño and West African rainfall with Atlantic major hurricane activity. *J. Climate*, **9**, 1169–1187, doi:10.1175/1520-0442(1996)009<1169:PMFTAO>2.0.CO;2.

——, C. W. Landsea, A. M. Mestas-Nuñez, and W. M. Gray, 2001: The recent increase in Atlantic hurricane activity: Causes and implications. *Science*, **293**, 474–479, doi:10.1126/science.1060040.

Gray, W. M., 1968: Global view of origin of tropical disturbances and storms. *Mon. Wea. Rev.*, **96**, 669–700, doi:10.1175/1520-0493(1968)096<0669:GVOTOO>2.0.CO;2.

Guba, O., M. A. Taylor, P. A. Ullrich, J. R. Overfelt, and M. N. Levy, 2014: The spectral element method (SEM) on variable-resolution grids: Evaluating grid sensitivity and resolution-aware numerical viscosity. *Geosci. Model Dev.*, **7**, 2803–2816, doi:10.5194/gmd-7-2803-2014.

Hart, R. E., R. N. Maue, and M. C. Watson, 2007: Estimating local memory of tropical cyclones through MPI anomaly evolution. *Mon. Wea. Rev.*, **135**, 3990–4005, doi:10.1175/2007MWR2038.1.

Hazelworth, J. B., 1968: Water temperature variations resulting from hurricanes. *J. Geophys. Res.*, **73**, 5105–5123, doi:10.1029/JB073i016p05105.

Holland, G. J., 1997: The maximum potential intensity of tropical cyclones. *J. Atmos. Sci.*, **54**, 2519–2541, doi:10.1175/1520-0469(1997)054<2519:TMPIOT>2.0.CO;2.

Huang, P., T. B. Sanford, and J. Imberger, 2009: Heat and turbulent kinetic energy budgets for surface layer cooling induced by the passage of Hurricane Frances (2004). *J. Geophys. Res.*, **114**, C12023, doi:10.1029/2009JC005603.

Huffman, G. J., and Coauthors, 2007: The TRMM Multisatellite Precipitation Analysis (TMPA): Quasi-global, multiyear, combined-sensor precipitation estimates at fine scales. *J. Hydrometeor.*, **8**, 38–55, doi:10.1175/JHM560.1.

Hurrell, J. W., J. J. Hack, D. Shea, J. M. Caron, and J. Rosinski, 2008: A new sea surface temperature and sea ice boundary dataset for the Community Atmosphere Model. *J. Climate*, **21**, 5145–5153, doi:10.1175/2008JCLI2292.1.

——, and Coauthors, 2013: The Community Earth System Model: A framework for collaborative research. *Bull. Amer. Meteor. Soc.*, **94**, 1339–1360, doi:10.1175/BAMS-D-12-00121.1.

Jansen, M. F., R. Ferrari, and T. A. Mooring, 2010: Seasonal versus permanent thermocline warming by tropical cyclones. *Geophys. Res. Lett.*, **37**, L03602, doi:10.1029/2009GL041808.

Jourdain, N. C., B. Barnier, N. Ferry, J. Vialard, C. E. Menkes, M. Lengaigne, and L. Parent, 2014: Tropical cyclones in two atmospheric (re)analyses and their response in two oceanic reanalyses. *Ocean Modell.*, **73**, 108–122, doi:10.1016/j.ocemod.2013.10.007.

Jullien, S., P. Marchesiello, C. Menkes, J. Lefèvre, N. Jourdain, G. Samson, and M. Lengaigne, 2014: Ocean feedback to tropical cyclones: Climatology and processes. *Climate Dyn.*, **43**, 2831–2854, doi:10.1007/s00382-014-2096-6.

Kalnay, E., and Coauthors, 1996: The NCEP/NCAR 40-year reanalysis project. *Bull. Amer. Meteor. Soc.*, **77**, 437–471, doi:10.1175/1520-0477(1996)077<0437:TNYRP>2.0.CO;2.

Kiehl, J. T., C. A. Shields, J. J. Hack, and W. D. Collins, 2006: The climate sensitivity of the Community Climate System Model version 3 (CCSM3). *J. Climate*, **19**, 2584–2596, doi:10.1175/JCLI3747.1.

Kim, H.-S., G. A. Vecchi, T. R. Knutson, W. G. Anderson, T. L. Delworth, A. Rosati, F. Zeng, and M. Zhao, 2014: Tropical cyclone simulation and response to CO_2 doubling in the GFDL CM2.5 high-resolution coupled climate model. *J. Climate*, **27**, 8034–8054, doi:10.1175/JCLI-D-13-00475.1.

Knapp, K. R., M. C. Kruk, D. H. Levinson, H. J. Diamond, and C. J. Neumann, 2010: The International Best Track Archive For Climate Stewardship (IBTrACS). *Bull. Amer. Meteor. Soc.*, **91**, 363–376, doi:10.1175/2009BAMS2755.1.

Knutson, T. R., R. E. Tuleya, W. Shen, and I. Ginis, 2001: Impact of CO_2-induced warming on hurricane intensities as simulated in a hurricane model with ocean coupling. *J. Climate*, **14**, 2458–2468, doi:10.1175/1520-0442(2001)014<2458:IOCIWO>2.0.CO;2.

Landman, W. A., A. Seth, and S. J. Camargo, 2005: The effect of regional climate model domain choice on the simulation of tropical cyclone–like vortices in the southwestern Indian Ocean. *J. Climate*, **18**, 1263–1274, doi:10.1175/JCLI3324.1.

Li, H., R. L. Sriver, and M. Goes, 2016: Modeled sensitivity of the Northwestern Pacific upper-ocean response to tropical cyclones in a fully coupled climate model with varying ocean grid resolution. *J. Geophys. Res.*, **121**, 586–601, doi:10.1002/2015JC011226.

Lin, I.-I., I.-F. Pun, and C.-C. Wu, 2009: Upper-ocean thermal structure and the western North Pacific category 5 typhoons. Part II: Dependence on translation speed. *Mon. Wea. Rev.*, **137**, 3744–3757, doi:10.1175/2009MWR2713.1.

Lloyd, I. D., and G. A. Vecchi, 2011: Observational evidence for oceanic controls on hurricane intensity. *J. Climate*, **24**, 1138–1153, doi:10.1175/2010JCLI3763.1.

Manganello, J. V., and Coauthors, 2012: Tropical cyclone climatology in a 10-km global atmospheric GCM: Toward weather-resolving

climate modeling. *J. Climate*, **25**, 3867–3893, doi:10.1175/JCLI-D-11-00346.1.

Mei, W., and C. Pasquero, 2013: Spatial and temporal characterization of sea surface temperature response to tropical cyclones. *J. Climate*, **26**, 3745–3765, doi:10.1175/JCLI-D-12-00125.1.

Morey, S. L., M. A. Bourassa, D. S. Dukhovskoy, and J. J. O'Brien, 2006: Modeling studies of the upper ocean response to a tropical cyclone. *Ocean Dyn.*, **56**, 594–606, doi:10.1007/s10236-006-0085-y.

Murakami, H., and Coauthors, 2012: Future changes in tropical cyclone activity projected by the new high-resolution MRI-AGCM. *J. Climate*, **25**, 3237–3260, doi:10.1175/JCLI-D-11-00415.1.

——, and Coauthors, 2015: Simulation and prediction of category 4 and 5 hurricanes in the high-resolution GFDL HiFLOR coupled climate model. *J. Climate*, **28**, 9058–9079, doi:10.1175/JCLI-D-15-0216.1.

Neale, R. B., and Coauthors, 2012: Description of the NCAR Community Atmosphere Model (CAM 5.0). NCAR Tech. Note NCAR/TN-486+STR, 268 pp.

Needham, H. F., B. D. Keim, and D. Sathiaraj, 2015: A review of tropical cyclone-generated storm surges: Global data sources, observations, and impacts. *Rev. Geophys.*, **53**, 545–591, doi:10.1002/2014RG000477.

Ogata, T., R. Mizuta, Y. Adachi, H. Murakami, and T. Ose, 2016: Atmosphere–ocean coupling effect on intense tropical cyclone distribution and its future change with 60 km-AOGCM. *Sci. Rep.*, **6**, 29800, doi:10.1038/srep29800.

Oleson, K., and Coauthors, 2010: Technical description of version 4.0 of the Community Land Model (CLM). NCAR Tech. Note NCAR/TN-478+STR, 257 pp., doi:10.5065/D6FB50WZ.

Oouchi, K., J. Yoshimura, H. Yoshimura, R. Mizuta, S. Kusunoki, and A. Noda, 2006: Tropical cyclone climatology in a global-warming climate as simulated in a 20 km-mesh global atmospheric model: Frequency and wind intensity analyses. *J. Meteor. Soc. Japan*, **84**, 259–276, doi:10.2151/jmsj.84.259.

Powell, M. D., P. J. Vickery, and T. A. Reinhold, 2003: Reduced drag coefficient for high wind speeds in tropical cyclones. *Nature*, **422**, 279–283, doi:10.1038/nature01481.

Price, J. F., 1981: Upper ocean response to a hurricane. *J. Phys. Oceanogr.*, **11**, 153–175, doi:10.1175/1520-0485(1981)011<0153:UORTAH>2.0.CO;2.

——, J. Morzel, and P. P. Niiler, 2008: Warming of SST in the cool wake of a moving hurricane. *J. Geophys. Res.*, **113**, C07010, doi:10.1029/2007JC004393.

Pun, I.-F., I.-I. Lin, and M.-H. Lo, 2013: Recent increase in high tropical cyclone heat potential area in the Western North Pacific Ocean. *Geophys. Res. Lett.*, **40**, 4680–4684, doi:10.1002/grl.50548.

Reed, K. A., J. T. Bacmeister, N. A. Rosenbloom, M. F. Wehner, S. C. Bates, P. H. Lauritzen, J. E. Truesdale, and C. Hannay, 2015: Impact of the dynamical core on the direct simulation of tropical cyclones in a high-resolution global model. *Geophys. Res. Lett.*, **42**, 3603–3608, doi:10.1002/2015GL063974.

Rienecker, M. M., and Coauthors, 2011: MERRA: NASA's Modern-Era Retrospective Analysis for Research and applications. *J. Climate*, **24**, 3624–3648, doi:10.1175/JCLI-D-11-00015.1.

Samson, G., H. Giordani, G. Caniaux, and F. Roux, 2009: Numerical investigation of an oceanic resonant regime induced by hurricane winds. *Ocean Dyn.*, **59**, 565–586, doi:10.1007/s10236-009-0203-8.

Santer, B. D., T. M. L. Wigley, and P. D. Jones, 1993: Correlation methods in fingerprint detection studies. *Climate Dyn.*, **8**, 265–276, doi:10.1007/BF00209666.

Satoh, M., and Coauthors, 2012: The intra-seasonal oscillation and its control of tropical cyclones simulated by high-resolution global atmospheric models. *Climate Dyn.*, **39**, 2185–2206, doi:10.1007/s00382-011-1235-6.

Schade, L. R., and K. A. Emanuel, 1999: The ocean's effect on the intensity of tropical cyclones: Results from a simple coupled atmosphere–ocean model. *J. Atmos. Sci.*, **56**, 642–651, doi:10.1175/1520-0469(1999)056<0642:TOSEOT>2.0.CO;2.

Scoccimarro, E., and Coauthors, 2011: Effects of tropical cyclones on ocean heat transport in a high-resolution coupled general circulation model. *J. Climate*, **24**, 4368–4384, doi:10.1175/2011JCLI4104.1.

Shay, L. K., P. G. Black, A. J. Mariano, J. D. Hawkins, and R. L. Elsberry, 1992: Upper ocean response to Hurricane Gilbert. *J. Geophys. Res.*, **97**, 20 227–20 248, doi:10.1029/92JC01586.

Simpson, R. H., 1974: The hurricane disaster—Potential scale. *Weatherwise*, **27**, 169–186, doi:10.1080/00431672.1974.9931702.

Small, R. J., and Coauthors, 2014: A new synoptic scale resolving global climate simulation using the Community Earth System Model. *J. Adv. Model. Earth Syst.*, **6**, 1065–1094, doi:10.1002/2014MS000363.

Sriver, R. L., and M. Huber, 2007: Observational evidence for an ocean heat pump induced by tropical cyclones. *Nature*, **447**, 577–580, doi:10.1038/nature05785.

Strachan, J., P. L. Vidale, K. Hodges, M. Roberts, and M.-E. Demory, 2013: Investigating global tropical cyclone activity with a hierarchy of AGCMs: The role of model resolution. *J. Climate*, **26**, 133–152, doi:10.1175/JCLI-D-12-00012.1.

Taylor, K. E., 2001: Summarizing multiple aspects of model performance in a single diagram. *J. Geophys. Res.*, **106**, 7183–7192, doi:10.1029/2000JD900719.

Taylor, M. A., and A. Fournier, 2010: A compatible and conservative spectral element method on unstructured grids. *J. Comput. Phys.*, **229**, 5879–5895, doi:10.1016/j.jcp.2010.04.008.

——, J. Tribbia, and M. Iskandarani, 1997: The spectral element method for the shallow water equations on the sphere. *J. Comput. Phys.*, **130**, 92–108, doi:10.1006/jcph.1996.5554.

Ullrich, P. A., and C. M. Zarzycki, 2016: TempestExtremes v1.0: A framework for scale-insensitive pointwise feature tracking on unstructured grids. *Geosci. Model Dev. Discuss.*, doi:10.5194/gmd-2016-217, in press.

Vecchi, G. A., and Coauthors, 2014: On the seasonal forecasting of regional tropical cyclone activity. *J. Climate*, **27**, 7994–8016, doi:10.1175/JCLI-D-14-00158.1.

Vincent, E. M., M. Lengaigne, G. Madec, J. Vialard, G. Samson, N. C. Jourdain, C. E. Menkes, and S. Jullien, 2012a: Processes setting the characteristics of sea surface cooling induced by tropical cyclones. *J. Geophys. Res.*, **117**, C02020, doi:10.1029/2011JC007396.

——, ——, J. Vialard, G. Madec, N. C. Jourdain, and S. Masson, 2012b: Assessing the oceanic control on the amplitude of sea surface cooling induced by tropical cyclones. *J. Geophys. Res.*, **117**, C05023, doi:10.1029/2011JC007705.

Walsh, K. J. E., M. Fiorino, C. W. Landsea, and K. L. McInnes, 2007: Objectively determined resolution-dependent threshold criteria for the detection of tropical cyclones in climate models and reanalyses. *J. Climate*, **20**, 2307–2314, doi:10.1175/JCLI4074.1.

——, and Coauthors, 2015: Hurricanes and climate: The U.S. CLIVAR working group on hurricanes. *Bull. Amer. Meteor. Soc.*, **96**, 997–1017, doi:10.1175/BAMS-D-13-00242.1.

Wang, C., L. Zhang, S.-K. Lee, L. Wu, and C. R. Mechoso, 2014: A global perspective on CMIP5 climate model biases. *Nat. Climate Change*, **4**, 201–205, doi:10.1038/nclimate2118.

Wehner, M. F., and Coauthors, 2014: The effect of horizontal resolution on simulation quality in the Community Atmospheric Model, CAM5.1. *J. Adv. Model. Earth Syst.*, **6**, 980–997, doi:10.1002/2013MS000276.

——, Prabhat, K. A. Reed, D. Stone, W. D. Collins, and J. T. Bacmeister, 2015: Resolution dependence of future tropical cyclone projections of CAM5.1 in the U.S. CLIVAR Hurricane Working Group idealized configurations. *J. Climate*, **28**, 3905–3925, doi:10.1175/JCLI-D-14-00311.1.

Young, I. T., 1977: Proof without prejudice: Use of the Kolmogorov–Smirnov test for the analysis of histograms from flow systems and other sources. *J. Histochem. Cytochem.*, **25**, 935–941, doi:10.1177/25.7.894009.

Zarzycki, C. M., and C. Jablonowski, 2014: A multidecadal simulation of Atlantic tropical cyclones using a variable-resolution global atmospheric general circulation model. *J. Adv. Model. Earth Syst.*, **6**, 805–828, doi:10.1002/2014MS000352.

——, M. N. Levy, C. Jablonowski, J. R. Overfelt, M. A. Taylor, and P. A. Ullrich, 2014: Aquaplanet experiments using CAM's variable-resolution dynamical core. *J. Climate*, **27**, 5481–5503, doi:10.1175/JCLI-D-14-00004.1.

——, C. Jablonowski, D. R. Thatcher, and M. A. Taylor, 2015: Effects of localized grid refinement on the general circulation and climatology in the Community Atmosphere Model. *J. Climate*, **28**, 2777–2803, doi:10.1175/JCLI-D-14-00599.1.

Zhao, M., I. M. Held, S. J. Lin, and G. A. Vecchi, 2009: Simulations of global hurricane climatology, interannual variability, and response to global warming using a 50-km resolution GCM. *J. Climate*, **22**, 6653–6678, doi:10.1175/2009JCLI3049.1.